IV. 研究成果の刊行物・別刷

Lnk regulates integrin αIIbβ3 outside-in signaling in mouse platelets, leading to stabilization of thrombus development in vivo

Hitoshi Takizawa,[1] Satoshi Nishimura,[2,3,4] Naoya Takayama,[5] Atsushi Oda,[6] Hidekazu Nishikii,[5] Yohei Morita,[5] Sei Kakinuma,[5] Satoshi Yamazaki,[5] Satoshi Okamura,[5] Noriko Tamura,[7] Shinya Goto,[7] Akira Sawaguchi,[8] Ichiro Manabe,[2,3,4] Kiyoshi Takatsu,[9] Hiromitsu Nakauchi,[5] Satoshi Takaki,[1] and Koji Eto[5]

[1]Research Institute, International Medical Center of Japan, Tokyo, Japan. [2]Department of Cardiovascular Medicine, Graduate School of Medicine and [3]Translational Systems Biology and Medicine Initiative, University of Tokyo, Tokyo, Japan. [4]PREST, Japan Science and Technology Agency, Tokyo, Japan. [5]Center for Stem Cell Biology and Regenerative Medicine, Institute of Medical Science, University of Tokyo, Tokyo, Japan. [6]Department of Environmental Medicine, Graduate School of Medicine, Hokkaido University, Sapporo, Japan. [7]Department of Medicine, Tokai University School of Medicine, Isehara, Japan. [8]Department of Anatomy, Faculty of Medicine, University of Miyazaki, Miyazaki, Japan. [9]Preferectural Institute for Pharmaceutical Research, Toyama, Japan.

The nature of the in vivo cellular events underlying thrombus formation mediated by platelet activation remains unclear because of the absence of a modality for analysis. Lymphocyte adaptor protein (Lnk; also known as Sh2b3) is an adaptor protein that inhibits thrombopoietin-mediated signaling, and as a result, megakaryocyte and platelet counts are elevated in *Lnk*$^{-/-}$ mice. Here we describe an unanticipated role for Lnk in stabilizing thrombus formation and clarify the activities of Lnk in platelets transduced through integrin αIIbβ3–mediated outside-in signaling. We equalized platelet counts in wild-type and *Lnk*$^{-/-}$ mice by using genetic depletion of Lnk and BM transplantation. Using $FeCl_3$- or laser-induced injury and in vivo imaging that enabled observation of single platelet behavior and the multiple steps in thrombus formation, we determined that Lnk is an essential contributor to the stabilization of developing thrombi within vessels. *Lnk*$^{-/-}$ platelets exhibited a reduced ability to fully spread on fibrinogen and mediate clot retraction, reduced tyrosine phosphorylation of the β3 integrin subunit, and reduced binding of Fyn to integrin αIIbβ3. These results provide new insight into the mechanism of αIIbβ3-based outside-in signaling, which appears to be coordinated in platelets by Lnk, Fyn, and integrins. Outside-in signaling modulators could represent new therapeutic targets for the prevention of cardiovascular events.

Introduction

Platelet activation is controlled through a series of highly regulated processes and is critical for maintaining normal homeostasis (1). The nature of hemostasis and thrombosis mediated in vivo by activated platelets and its contribution to cardiovascular events remains unclear, however. Particularly challenging has been the characterization of the multicellular network of interactions among platelets, endothelial cells, leukocytes, and erythrocytes that occur during thrombus formation in pathological settings and analysis of the kinetics of platelet activity. Injury to vascular endothelial cells exposes matrix proteins, which induce platelets to adhere to the vessel wall, where they subsequently spread and become activated. At the high shear rates found within the circulation, vWF immobilized on the vessel wall binds to the platelet receptor glycoprotein Ib-V-IX complex (GPIb-V-IX), facilitating platelet adhesion to injured sites, where collagen and/or laminin are exposed (2, 3). Once activated, the adhering platelets secrete soluble mediators to recruit additional circulating platelets, and, through their aggregation, bleeding is stopped. Platelet activation is mediated via several signaling pathways, including the integrin αIIbβ3 pathway (1). Other receptor-ligand interactions, including the binding of GPVI-collagen, $P2Y_1$/$P2Y_{12}$-ADP, and protease-activated G protein–coupled receptor–thrombin (PAR-thrombin), synergistically promote integrin αIIbβ3 activation (inside-out signaling) and the subsequent binding of fibrinogen or vWF to integrin αIIbβ3. This binding triggers signaling that promotes cytoskeletal changes that lead to the spread and stabilization of platelet thrombi through a process termed outside-in signaling (1, 2).

It is also known that αIIbβ3 physically interacts with non–receptor tyrosine kinases such as Src and Syk (4, 5) and that activation of these kinases upon engagement of integrin with fibrinogen contributes to the stability of thrombi in vivo (6). The kinases and adaptors involved in the assembly of the αIIbβ3-based signaling complex are believed to include Syk, lymphocyte cytosolic protein 2 (Lcp2, also known as SH2 domain–containing leukocyte protein of 76 kDa [SLP-76]), Vav, and Fyn-binding protein (Fyb, also known as adhesion and degranulation promoting adaptor protein [ADAP]) (4, 5). Tyrosine phosphorylation of the cytoplasmic domain of the integrin β3 subunit, at least on Tyr747, is required for stable platelet aggregation and the interaction of myosin with the β3 subunit in platelets (7), which is believed to be necessary for full clot retraction (8–10).

Lnk (SH2B adaptor protein 3 [Sh2b3]) belongs to the Src-homology 2 (SH2) adaptor family, which also includes SH2-B (Sh2b1) and adaptor protein with PH and SH2 domains (APS; Sh2b2) (11).

Authorship note: Hitoshi Takizawa and Satoshi Nishimura contributed equally to this work.

Conflict of interest: The authors have declared that no conflict of interest exists.

Citation for this article: *J. Clin. Invest.* doi:10.1172/JCI39503.

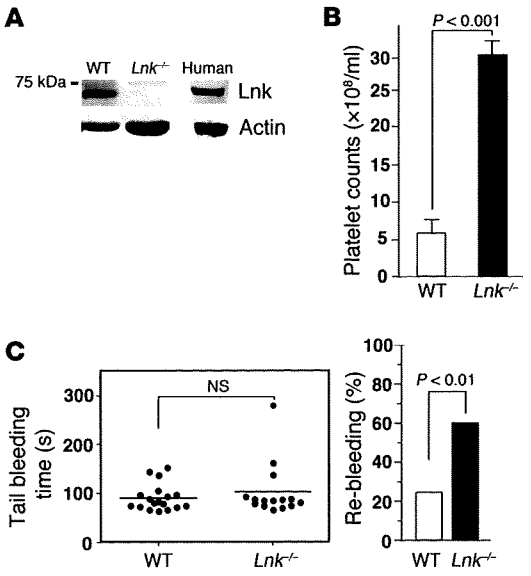

Figure 1
Increased numbers of platelets circulate in *Lnk*$^{-/-}$ mice, but re-bleeding events are increased, while bleeding times are comparable. (**A**) Lnk levels in platelets. Washed platelets from WT and *Lnk*$^{-/-}$ mice or human platelets were lysed and were subjected to immunoblotting with anti-Lnk and anti-actin Abs. (**B**) Platelet counts in EDTA-treated peripheral blood (mean ± SD, n = 15 each). (**C**) Tails of WT (n = 18) and *Lnk*$^{-/-}$ mice (n = 15) were warmed and then transected, immersed in PBS at 37°C, and then monitored for 60 seconds so that any re-bleeding would be detected (detection was positive or negative). Horizontal bars in the left panel show mean in each group.

Lnk-deficient (*Lnk*$^{-/-}$) mouse strains exhibit excessive accumulation of c-Kit^{+}Sca-1^{+}lineage^{-} (KSL) CD34$^{-/lo}$ HSCs, B cell precursors, erythroblasts, megakaryocytes, and platelets but do not exhibit thrombogenesis and have normal longevity (11–14). The observed phenotypes of *Lnk*$^{-/-}$ mice are caused by a loss of negative regulation by Lnk signaling transduced through several growth factor and cytokine receptors, including the stem cell factor receptor c-Kit, the erythropoietin receptor, and the thrombopoietin receptor c-Mpl (11, 12, 14–17). In the present study, we used an $FeCl_3$-induced injury model and our high-resolution imaging system, which enables observation of single platelet behavior in vivo (18), to examine the function of Lnk in platelets with the aim of clarifying its role in thrombosis. Our results suggest that Lnk promotes stabilization of the developed thrombus, mainly through integrin αIIbβ3-mediated actin cytoskeletal reorganization, and suggest this molecule may represent a new therapeutic target for the treatment and/or prevention of cardiovascular disease.

Results

Thrombus stability is impaired in Lnk$^{-/-}$ *mice in different mouse models of thrombosis.* Lnk is expressed by megakaryocytes, where it acts through integrin signaling to regulate their growth and maturation (14, 19). To determine whether platelets retain Lnk after their release from megakaryocytes and, if so, what its function is, we first used immunoblotting to assess Lnk levels in platelets obtained from WT C57BL/6 mice. This analysis confirmed that substantial amounts of Lnk are retained by WT platelets, and similar results were obtained in humans (Figure 1A). Accordingly, we next investigated the function of Lnk in platelets by examining the effect of Lnk deficiency. As reported previously (14, 19), *Lnk*$^{-/-}$ mice showed a 5-fold increase in platelet number (Figure 1B), though flow cytometry revealed platelet size to be unaffected by the absence of Lnk (data not shown). Moreover, transmission electron microscopic examination revealed that the intracellular structures of resting WT and *Lnk*$^{-/-}$ platelets, including the α- and dense granules, were indistinguishable (Supplemental Figure 1A; supplemental material available online with this article; doi:10.1172/JCI39503DS1). Likewise, the expression levels of the major integrin subunits, αIIb, α2, β3, and β1, as well as GPIbα (the vWF receptor) and GPVI (the collagen receptor), were also similar in WT and *Lnk*$^{-/-}$ platelets (Supplemental Figure 1B).

To examine the functional consequences of Lnk deficiency in mice, we inflicted tail wounds on the mice, after which *Lnk*$^{-/-}$ mice exhibited bleeding times that were comparable to those in WT mice. But whereas 23% of WT mice showed re-bleeding, 60% of *Lnk*$^{-/-}$ mice re-bled ($P < 0.01$ in a χ^2 test, Figure 1C; re-bleeding times did not differ significantly: WT, 58 ± 8 seconds vs. *Lnk*$^{-/-}$, 62 ± 6 seconds), suggesting that thrombi formed in *Lnk*$^{-/-}$ mice are more fragile than those formed in WT mice (1, 8, 20).

To accurately interpret the results summarized above, 2 characteristics of the system had to be taken into account: (a) the numbers of circulating platelets in *Lnk*$^{-/-}$ mice were 5-fold higher than in WT mice (Figure 1B); and (b) Lnk is expressed in endothelial cells as well as platelets (21). In order to exclude the influence of endothelial cells and platelet number, we performed BM transplantation using WT or *Lnk*$^{-/-}$ BM cells. Because it is well established that Lnk deficiency increases stem cell number and enhances the engraftment efficiency upon transplantation (22), we transplanted 1×10^7 BM cells from Ly5.1 WT mice or 2×10^5 or 5×10^5 BM cells from Ly5.1 *Lnk*$^{-/-}$ mice into irradiated 8-week-old Ly5.2 recipient mice, which are hereafter referred to as WT-chimeras and Lnk-chimeras, respectively (Figure 2A). We confirmed that with successful BM replacement (all mice used showed greater than 98% chimerism at Ly5.1/Ly5.2 on myeloid-lineage cells) and with platelets lacking Lnk expression from Lnk-chimeras, the platelet counts in 16-week-old WT-chimeras (8 weeks after transplantation) were comparable to those in 12-week-old Lnk-chimeras (4 weeks after transplantation). By 8 weeks after transplantation, the Lnk-chimeras showed higher platelet counts (Figure 2B). Correspondingly, when compared with WT-chimeras at 8 weeks after transplantation, bleeding times were significantly prolonged in Lnk-chimeras at 4 weeks but not at 8 weeks ($P < 0.01$, Figure 2B). WT-chimeras at 8 weeks, Lnk-chimeras at 4 weeks, and Lnk-chimeras at 8 weeks showed re-bleeding times of 59 seconds (3 of 14 mice), 246 seconds (7 of 14 mice), and 57 seconds (5 of 11 mice), respectively. This suggests that the Lnk deficiency itself contributes to the increased tail bleeding and re-bleeding times. Although there was a high inverse correlation between bleeding times and platelet counts in both

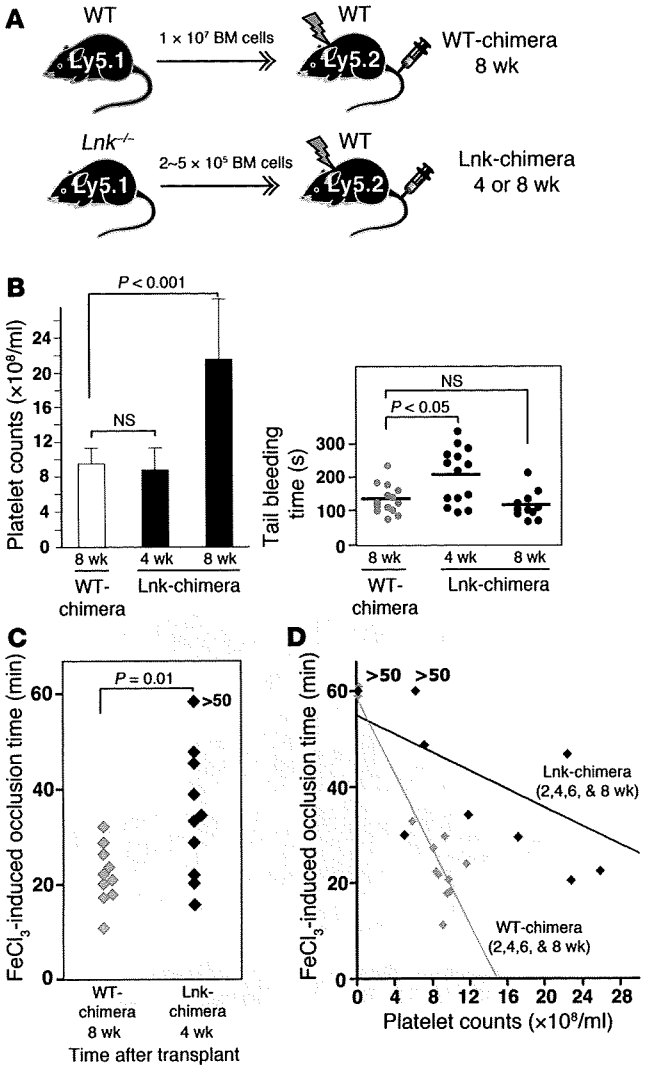

Figure 2
Adjustment of platelet counts through BM transplantation showed prolonged bleeding and occlusion times in a $FeCl_3$-induced thrombosis model. (**A**) The protocol for BM transplantation. (**B**) The left panel shows the platelet counts after transplantation (n = 11–14); data represent mean ± SD. The right panel shows the duration of tail bleeding at the indicated time points; horizontal bars show mean in each group. (**C**) Platelet counts in BM-transplanted mice. WT-chimeras at 8 weeks and Lnk-chimeras at 4 weeks after transplantation were utilized to measure occlusion times during $FeCl_3$-induced thrombosis in carotid arteries (WT-chimera, n = 10; Lnk-chimera, n = 10; P = 0.01). (**D**) Relationship between occlusion times with $FeCl_3$-induced thrombosis and platelet counts in WT- and Lnk-chimeras measured 2, 4, 6, and 8 weeks after transplantation (n = 12 animals in each group). Black symbols denote Lnk-chimeras, while gray ones denote WT-chimeras; the black ($y = -0.96x + 55.0$) and gray lines ($y = -3.94x + 58.6$) are fitted to the data from the Lnk- and WT-chimeras, respectively.

WT- and Lnk-chimeras, irrespective of platelet age or circulating platelet counts (Supplemental Figure 2), the results again suggest that the impaired thrombosis reflects the Lnk deficiency.

We then evaluated occlusion times in carotid arteries exposed to $FeCl_3$ (10% solution on the adventitial side) to induce endothelial injury for assessing thrombus formation in vivo (23). We found that in WT- and Lnk-chimeras with comparable platelet counts, occlusion times were significantly longer in the Lnk-chimeras, which is also indicative of a functional defect in $Lnk^{-/-}$ platelets (WT-chimera, n = 10; Lnk-chimera, n = 10; P = 0.01, Figure 2C). When we analyzed for the relationship between occlusion times and platelet counts in the chimeras 2, 4, 6, and 8 weeks after transplantation, there was a high inverse correlation between occlusion times and platelet counts. Of note, however, Lnk-chimeras exhibited longer occlusion times than WT-chimeras with similar platelet counts (Figure 2D), further confirming that Lnk deficiency impairs thrombus formation.

To assess the functionality of $Lnk^{-/-}$ platelets in more detail, we used a direct visual technique that enabled us to evaluate in vivo thrombus stability with much greater temporal and spatial resolution and to characterize the kinetics of $Lnk^{-/-}$ platelet activity involved in thrombus formation. This method is based on confocal laser microscopy and permits high spatiotemporal resolution of individual platelets under flow conditions in mesenteric capillaries and arterioles (24). With this system, laser irradiation produces ROS, which cause injury to the endothelial layer of the vessels (18). Because laser-induced thrombosis reportedly differs from the $FeCl_3$-induced injury model in terms of the mechanism of thrombus formation (25, 26), we again used WT-chimeras 8 weeks after transplantation and Lnk-chimeras 4 weeks after transplantation, as we did in the experiments shown in Figure 2C. We found that WT- and Lnk-chimeras showed similar single platelet kinetics in the absence of injury, including transient interactions with the endothelium (data not shown). After laser-induced injury, however, thrombus formation was severely diminished in the Lnk-chimeras.

After laser-induced injury to mesenteric capillaries, platelets adhered to the vessel walls at similar rates in the WT- and Lnk-chimeras (WT-chimeras, 1.59 ± 0.18 platelets/ms/μm vs. Lnk-chimeras, 1.48 ± 0.19 platelets/ms/μm; n = 30 vessels from 5 animals, P = 0.44). In the WT-chimeras, the adherent platelets caused platelets in the flowing blood to acutely pile up, and the resultant thrombus reduced the vessel lumen diameter and blood flow velocity. Ultimately, the blood vessel was completely occluded by plugged erythrocytes and/or leukocytes. By contrast, in the Lnk-chimeras, platelets adhered to the vessel wall more loosely than in WT-chimeras, so that they were frequently washed away by the blood flow. As a consequence, the number of platelets that piled up and the size of the resultant thrombus were smaller than in WT-chimeras (Figure 3A and Supplemental Videos 1 and 2). More intriguingly, in both Lnk- and WT-chimeras 2, 4, 6, and 8 weeks after transplantation, the number of platelets adhering to the vessel walls during thrombus formation appeared to be well correlated with the circulating platelet count. However, when we compared thrombus formation in Lnk- and WT-chimeras with similar platelet counts, there was a tendency for animals with $Lnk^{-/-}$ platelets (Lnk-chimeras) to show impaired thrombus formation, as compared with WT-chimeras. Moreover, the greatly increased platelet numbers in $Lnk^{-/-}$ animals did not enhance thrombus formation to levels similar to those seen in WT-chimeras (Figure 3B), which suggests that Lnk deficiency is itself a factor that contributes to the impaired stabilization of developing thrombi in our laser-induced injury model.

We also applied the laser-induced injury model to compare thrombosis in mesenteric capillaries and arterioles of 12-week-old

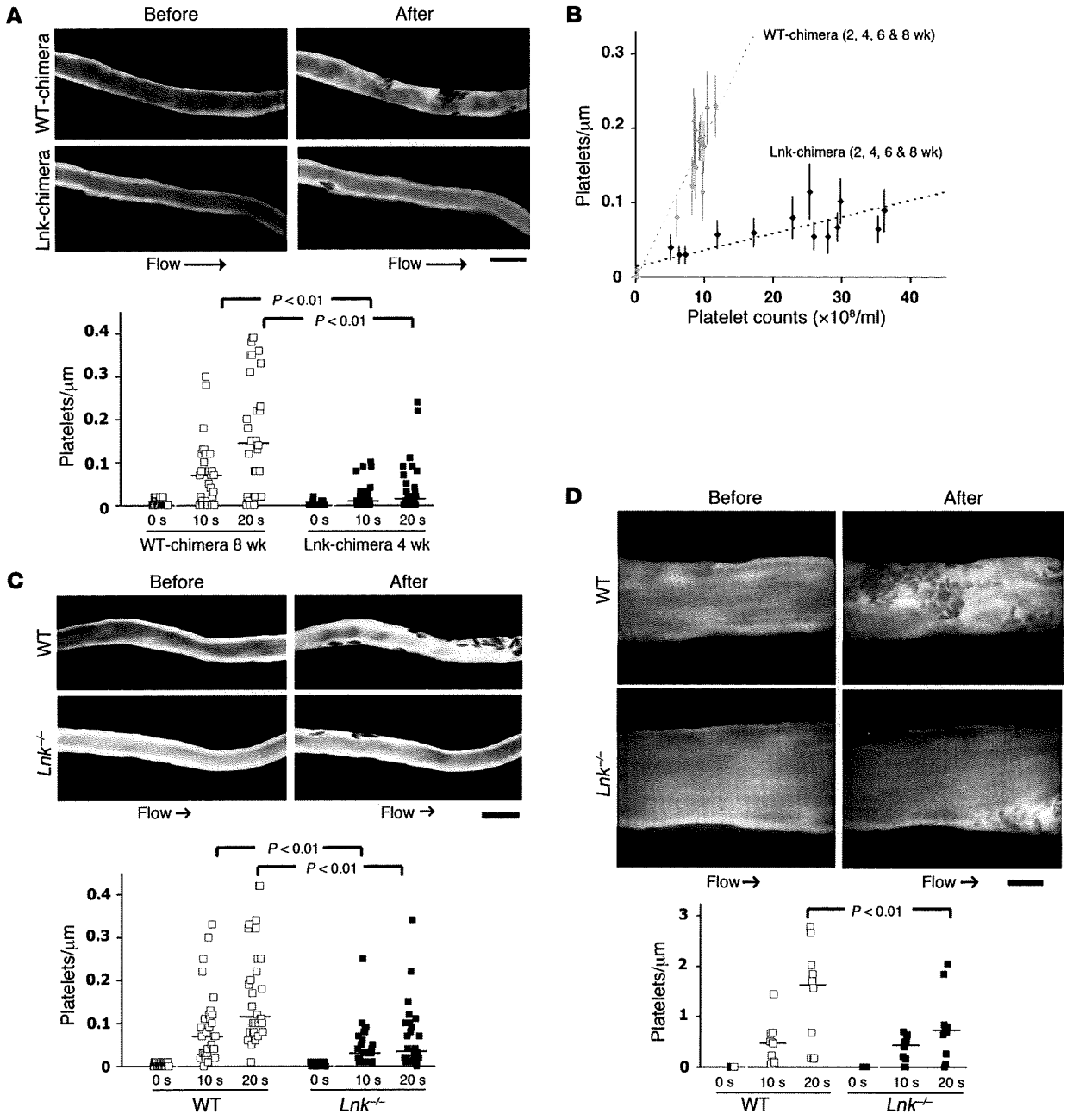

Figure 3

In vivo thrombus formation was impaired in Lnk-chimeras and *Lnk*$^{-/-}$ mice in a laser-induced injury model. (**A**, **C**, and **D**) Video stills of mesenteric capillaries (**A** and **C**) and arterioles (**D**) obtained using intravital fluorescence microscopy before and 20 seconds after laser-induced injury. The numbers of platelets in developing thrombi after laser injury to capillaries (**A** and **C**, lower panel) and arterioles (**D**, lower panel) were calculated. In **A**, **C**, and **D**, *y* axes represent the numbers of platelets per micrometer of observed vessel length. In **A**, results from WT-chimeras 8 weeks after transplantation (16 weeks old) and Lnk-chimeras 4 weeks after transplantation (12 weeks old) are shown ($n = 5$ each). (**B**) Relationship between platelet counts and laser-induced thrombosis. All recipient mice were studied 2, 4, 6, or 8 weeks after transplantation ($n = 17$ animals for each groups). For each mouse, the numbers of platelets per micrometer contributing to thrombi after 20-second injuries to 10 mesenteric capillaries are shown as mean ± SEM along with platelet count. Black and gray dotted lines are fitted to the data from the Lnk- and WT-chimeras, respectively. (**C** and **D**) Results from 12-week-old WT and *Lnk*$^{-/-}$ mice ($n = 5$ each). See Supplemental Videos 1–6 for original movies. Note the impaired thrombus formation in *Lnk*$^{-/-}$ mice in both capillaries and arterioles. Scale bars: 10 μm. Horizontal lines indicate the median values in **A**, **C**, and **D**.

WT and *Lnk*$^{-/-}$ mice (Figure 3, C and D, for capillaries and arterioles, respectively). Upon laser-induced injury, the platelet kinetics in *Lnk*$^{-/-}$ mice were similar to those seen in the Lnk-chimeric mice 4 weeks after transplantation. Initial attachment of the platelets to the vessel wall was observed; however, stable thrombus formation, including the piling up of platelets, was diminished in manner similar to that seen in the Lnk-chimeras. As a result, the numbers of platelets making up the thrombi were significantly reduced in

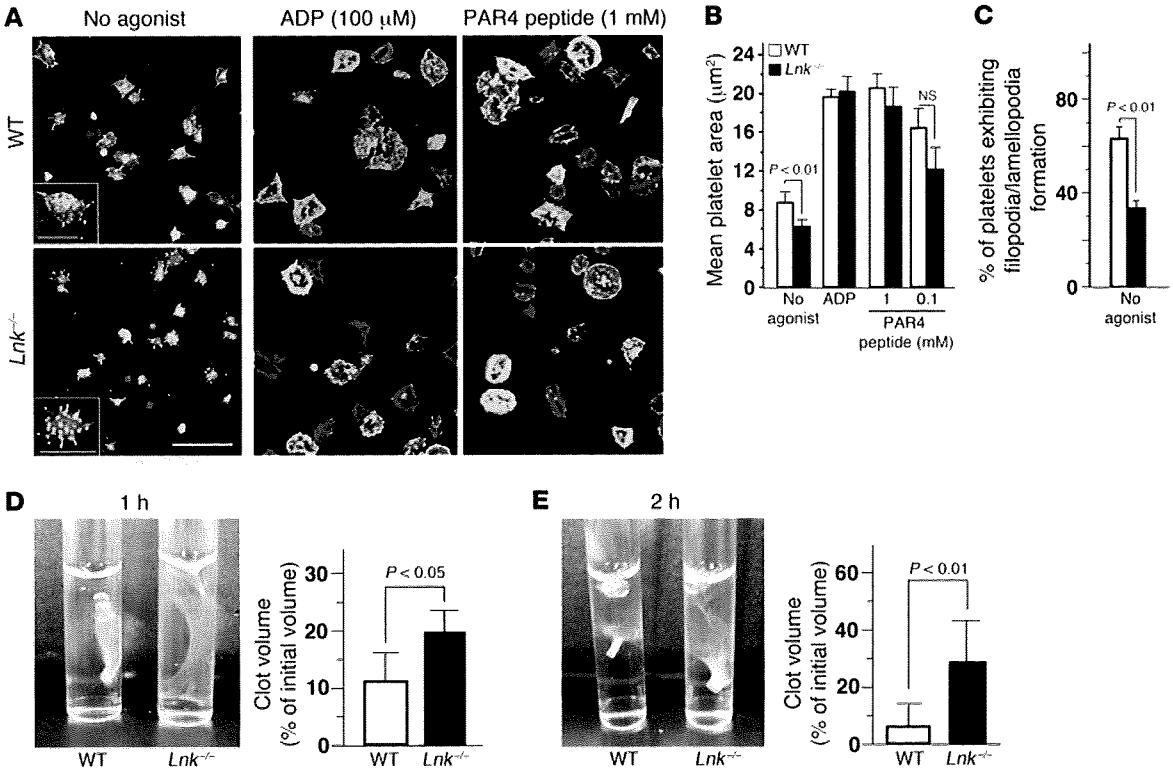

Figure 4

Lnk$^{-/-}$ platelets show defective αIIbβ3-dependent spreading on fibrinogen and fibrin clot retraction. (**A**) Washed platelets from WT and *Lnk*$^{-/-}$ mice were plated on fibrinogen-coated coverslips for 45 minutes. In some preparations, 100 μM ADP or 0.1 or 1 mM PAR4 receptor–activating peptide was present. Cells were fixed, permeabilized, and stained with rhodamine-phalloidin to visualize F-actin (red) and with anti-phosphotyrosine mAb (green). Scale bars: 10 μm (white); 4 μm (insets, orange). (**B**) Platelet spreading was quantified by computer analysis of their surface areas. Each bar in **B** represents the value (mean ± SD) from at least 250 platelets. (**C**) Percentages of platelets exhibiting filopodia or lamellipodia. Twenty sections (20–30 cells/section) were analyzed, and mean ± SD is shown. (**D** and **E**) Fibrin clot retraction was assessed at 1 and 2 hours after addition of thrombin, fibrinogen, and $CaCl_2$ to washed platelets from WT or *Lnk*$^{-/-}$ mice. The images show representative results at 1 (**D**) and 2 hours (**E**). The graphs show the summarized results at 1 (**D**) and 2 hours (**E**) (mean ± SD, $n = 10$ each).

both mesenteric capillaries (Figure 3C and Supplemental Videos 3 and 4) and arterioles (Figure 3D and Supplemental Videos 5 and 6). Taken together, the results indicate that the observed phenotype for thrombus formation caused by the Lnk deficiency is attributable to platelet function, per se, and does not reflect changes in endothelial cell function. This is noteworthy, as it suggests that there could be less thrombus formation in the Lnk-chimeras than in *Lnk*$^{-/-}$ mice, as the higher platelet counts in the latter might slightly compensate for their diminished functionality (Figure 3, A–C).

Lnk promotes integrin αIIbβ3-mediated actin cytoskeletal reorganization but not agonist-dependent integrin activation. To determine the basis for the instability of thrombi formed by *Lnk*$^{-/-}$ platelets, we examined their ability to adhere to fibrinogen-coated plates and their morphology after spreading, both of which are dependent on outside-in αIIbβ3 signaling (1, 8, 27). The initial adhesion of *Lnk*$^{-/-}$ platelets to fibrinogen-coated plates in the absence of agonistic stimuli appeared normal, as did formation of filopodial projections (data not shown). On the other hand, their subsequent spreading (after 15 minutes) was impaired, and formation of a lamellipodial edge was incomplete (shown at 45 minutes, Figure 4A, "No agonist") (28, 29). The mean area covered by the adhering platelets and the percentage of platelets showing filopodia and/or lamellipodia (percentage of spreading) were both significantly reduced in the absence of Lnk (at 45 minutes, Figure 4, B and C; time-dependent change in mean area without agonist, Supplemental Figure 3A). This suboptimal spreading of *Lnk*$^{-/-}$ platelets was not observed when they were stimulated with a high concentration of a G protein–coupled receptor agonist such as 100 μM ADP or 1 mM PAR4-activating peptide (sequence: AYPGKF) (Figure 4, A and B), although lower concentrations of agonists, such as 0.1 mM PAR4-activating peptide (Figure 4B) or 0.05 U/ml thrombin (Supplemental Figure 3B), did not completely restore the spreading on immobilized fibrinogen impaired by Lnk deficiency, even when the secretion of effectors from platelet granules was blocked (Supplemental Figure 3B). In addition, there was no significant difference in the reduction in the spread areas of platelets from Lnk-chimeras 4 weeks and 8 weeks after transplantation (data not shown), indicating that the impaired spreading caused by Lnk deficiency is independent of platelet age after myelosuppression. Thus, Lnk appears to continuously participate in a subset of αIIbβ3- and actin-dependent morphological responses triggered by platelet adhesion to fibrinogen (1) independently of its negative impact on proliferation in HSCs and megakaryocytes (12, 14, 19).

Another platelet response that is dependent on αIIbβ3 and the actin cytoskeleton is fibrin clot retraction (8, 9, 27), which we examined using equal numbers of *Lnk*$^{-/-}$ and WT washed platelets

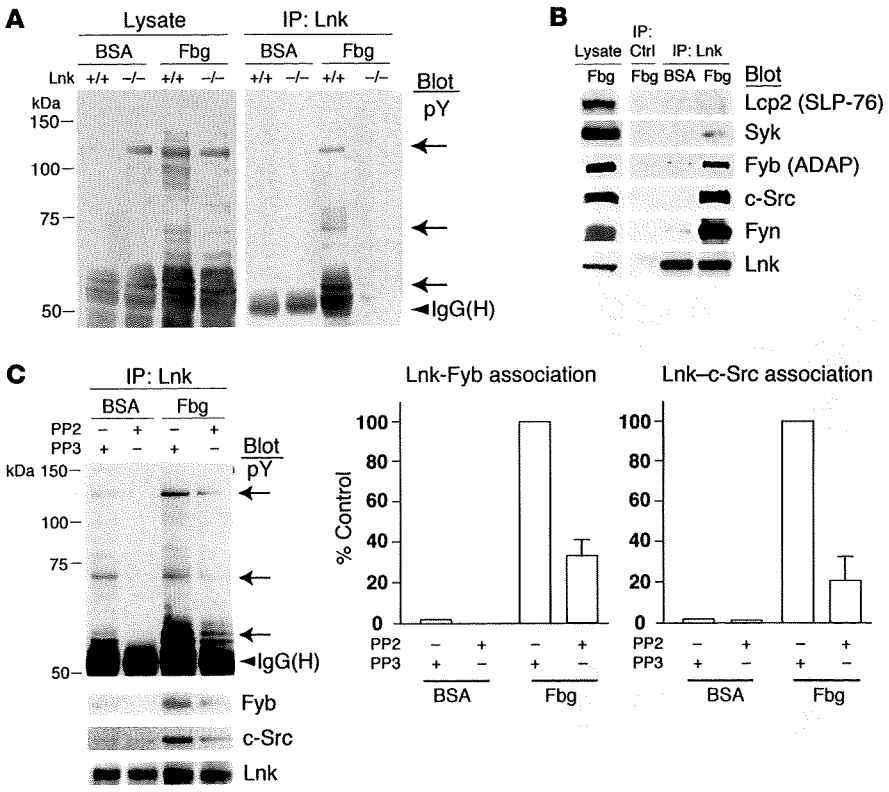

Figure 5
Lnk associates with c-Src, Fyn, and Fyb in a manner dependent on outside-in signaling. (**A**) Washed platelets from WT and *Lnk*$^{-/-}$ mice were plated on fibrinogen (Fbg) for 45 minutes or maintained in suspension in a BSA-coated dish. Platelet lysate (left) or proteins immunoprecipitated using anti-Lnk Abs (right, IP: Lnk) were separated and probed with anti-phosphotyrosine (pY) mAb. (**B**) Lysates from WT platelets prepared as in **A** and immunoprecipitates obtained using irrelevant control rabbit sera (IP: Ctrl) or anti-Lnk (IP: Lnk) were probed by immunoblotting for the indicated proteins. (**C**) WT platelets were incubated with 5 μM PP2 to block Src kinase activity or with PP3, an inactive congener of PP2. PP2 but not PP3 diminished tyrosine phosphorylation of cellular proteins and the association of c-Src and Fyb, with Lnk in platelets adhering to fibrinogen. The observation was confirmed using 20 μM SU6656, an unrelated selective c-Src inhibitor (data not shown). Arrows indicate bands for the expected phosphoproteins corresponding to Fyb, Lnk, and c-Src. Results shown are representative of 3 independent experiments. The 2 panels on the right show the quantification of Western blot bands from 3 experiments (mean ± SD). Maximal band density was defined as 100%.

in the presence of fibrinogen, $CaCl_2$, and thrombin (Figure 4, D and E). Under these conditions, the clot retraction seen with *Lnk*$^{-/-}$ platelets was slower and less effective than that seen with WT platelets, which is consistent with the idea that platelet responses are dependent on αIIbβ3-mediated actin cytoskeletal signaling and that Lnk is involved. To further study the role of αIIbβ3 activation in *Lnk*$^{-/-}$ platelets, we also used flow cytometry to quantify the specific binding of Alexa Fluor 488–conjugated fibrinogen to washed platelets upon stimulation with various concentrations of ADP, epinephrine, PAR4 peptide, phorbol myristate acetate, or convulxin (CVX), which selectively stimulates GPVI (Supplemental Figure 4A). We found that *Lnk*$^{-/-}$ and WT platelets showed similar fibrinogen binding, irrespective of the agonist inducing the inside-out signaling. In addition, levels of P-selectin expression were indistinguishable (Supplemental Figure 4B), suggesting that Lnk is not involved in α-granule secretion.

Lnk recruitment to the αIIbβ3-based signaling complex is dependent on outside-in signaling and c-Src activation. To understand the mechanism by which Lnk regulates outside-in signaling, we sought the molecule(s) that associates with Lnk in platelets. One prominent cellular event required for integrin-dependent responses is tyrosine phosphorylation of several cytosolic proteins (Figure 5A) (1, 4, 27). Incubation of WT platelets on fibrinogen induced tyrosine phosphorylation of cellular proteins with molecular weights of 60, 65–75, 90–110, and 120–130 kDa, but much less post-engagement tyrosine-phosphorylation was seen in *Lnk*$^{-/-}$ platelets. In addition, immunoprecipitation assays revealed that several phosphoproteins associate with Lnk (the 68-kDa protein was likely Lnk itself). A variety of proteins, including Syk, LCP2, and Fyb, are known to be tyrosine phosphorylated in an Src-dependent manner in fibrinogen-adherent platelets (29, 30). In the present study, both c-Src and Fyb co-immunoprecipitated with Lnk from WT platelets adhering to fibrinogen but not from unstimulated ones; Syk was only weakly detectable, and LCP2 was barely so (Figure 5B). It has also been proposed that Fyn, an Src-family protein, may contribute to integrin αIIbβ3 signaling (9, 20), and we found that, like c-Src, Fyn associated with Lnk in stimulated platelets (Figure 5B).

c-Src and Fyn are known to associate with the cytoplasmic tail of the integrin β3 subunit in vitro (20, 31), which suggests that after platelets bind to fibrinogen, Lnk regulates the assembly of an αIIbβ3-based signaling complex (5). We therefore asked whether the observed association of c-Src and/or Fyb with Lnk is dependent on Src kinase activity. When platelets were incubated with 5 μM PP2 (to block Src kinase activity) or PP3 (an inactive congener of PP2), PP2 but not PP3 diminished tyrosine phosphorylation of cellular proteins and the association of c-Src and Fyb with Lnk in platelets adhering to fibrinogen (Figure 5C). To then confirm that the phosphorylation of Lnk and its association with c-Src are dependent on c-Src activation, we used a COS7 cell expression system to evaluate the interaction in more detail (Supplemental Figure 5A). Flag-tagged WT Lnk (WT-Lnk) or a mutant form lacking the C-terminal portion containing Tyr536 (ΔC-Lnk) was expressed in COS7 cells in the presence and absence of a constitutively active form of human c-Src (Y530F, CA-Src). Whereas WT-Lnk became tyrosine phosphorylated when coexpressed with CA-Src, ΔC-Lnk showed little or no phosphorylation, indicating that Tyr536 is a key target site for phosphorylation by c-Src (Supplemental Figure 5A). On the other hand, a constitutively active form of Fyn did not phosphorylate WT-Lnk (data not shown). We then evaluated the consequences of the loss of c-Src–mediated Lnk phosphorylation using CHO cells, which constitutively express human αIIbβ3 (29, 32) and were previously shown to spread on immobilized fibrino-

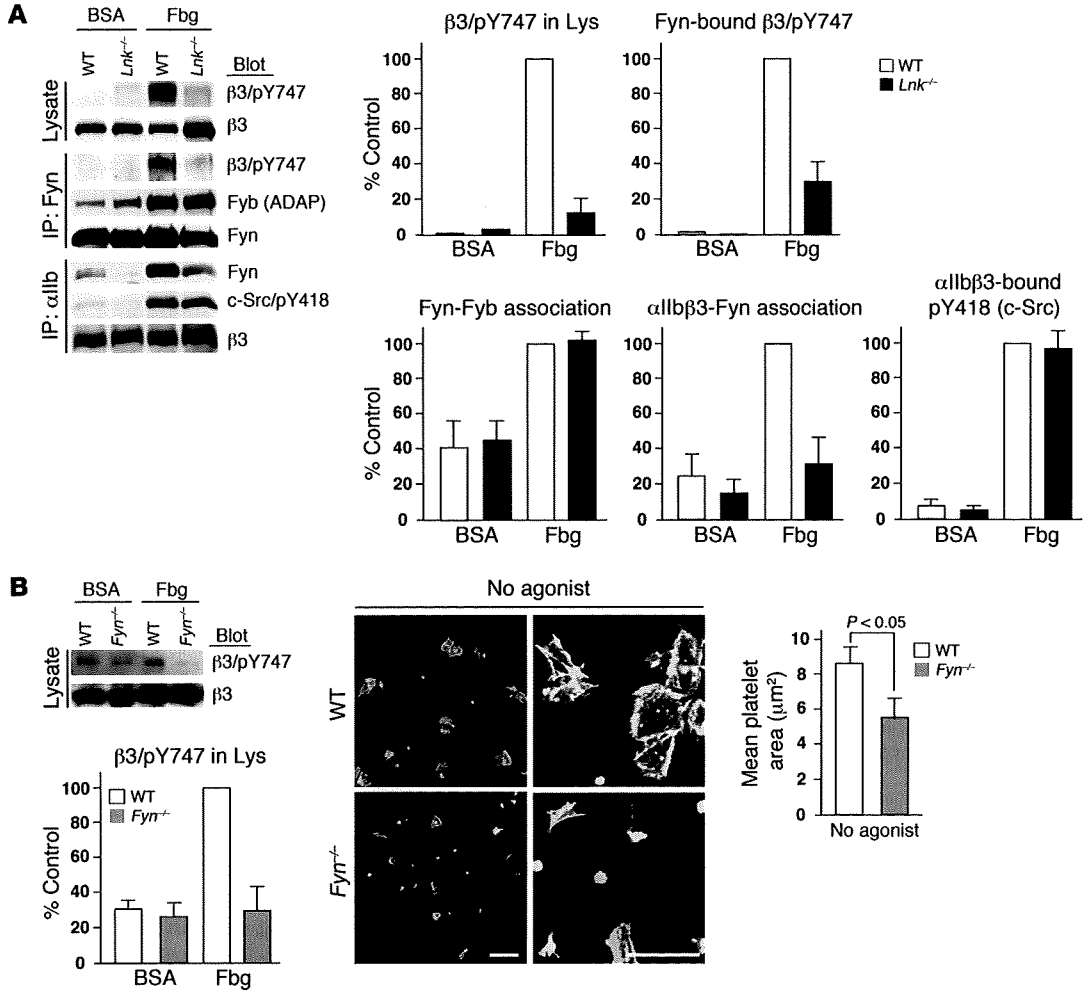

Figure 6

Lnk deficiency in platelets leads to reduced binding of Fyn to αIIbβ3 and reduced tyrosine phosphorylation of the cytoplasmic domain of the β3 integrin subunit. (**A**) WT and *Lnk*$^{-/-}$ platelets plated or maintained in suspension as in Figure 5A were lysed and analyzed by immunoblotting using anti–β3 integrin or anti–β3/p-Tyr747. In other sets, immunoprecipitation was elicited with anti-Fyn or anti-αIIb Ab. Each immunoblot panel is representative of 3 or 4 independent experiments, and estimated band densities are shown in the graphs. Band densities for WT samples from adherent platelets on fibrinogen were defined as 100%. Lys, lysates. (**B**) Washed platelets from WT and *Fyn*$^{-/-}$ mice were plated on fibrinogen for 45 minutes or maintained in suspension in a BSA-coated dish, lysed, and analyzed. The error bars in **A** and **B** indicate mean ± SD. (**C**) Left panels show the features of WT or *Fyn*$^{-/-}$ platelets allowed to spread on fibrinogen-coated coverslips for 45 minutes in the absence of agonist. The cells were fixed, permeabilized, and stained with Alexa 488 Fluor–phalloidin to visualize F-actin. Scale bars: 10 μm. The graph shows spreading quantified by computer analysis of their surface areas (mean ± SD).

gen in an Src kinase–dependent manner (32). When WT-Lnk or ΔC-Lnk was expressed as a GFP fusion protein, CHO cells expressing ΔC-Lnk showed fewer lamellipodia on fibrinogen than those expressing WT-Lnk (Supplemental Figure 5B). Thus, the absence of its C terminus again disrupted Lnk's ability to mediate formation of lamellipodia (Supplemental Figure 5B). Apparently, the C-terminal portion of Lnk and phosphorylation of Tyr536, which is likely regulated by c-Src, are key contributors to formation of lamellipodia and cell spreading mediated via integrin αIIbβ3.

Adherent Lnk$^{-/-}$ *platelets show reduced tyrosine phosphorylation of the β3 integrin subunit and reduced association of Fyn with αIIbβ3.* The importance of Src activation to outside-in αIIbβ3 signaling is well documented (4, 5, 31). Because Lnk appears to co-immunoprecipitate with both c-Src and Fyn (Figure 5B), we next asked whether Lnk might regulate the function of these kinases in platelets. During platelet aggregation or adhesion to fibrinogen, 2 conserved tyrosine residues in the β3 subunit, Tyr747 and Tyr759, are putatively targeted by Fyn, which is reportedly indispensable for clot retraction and prevention of re-bleeding from tail wounds (1, 8, 9). Moreover, Tyr747 is reportedly required for the binding of talin, filamin, c-Src, and other proteins essential for normal integrin signaling in platelets (33). We previously observed prominent phosphorylation of Tyr747 in WT platelets upon adherence to fibrinogen (10), but this response was severely impaired in *Lnk*$^{-/-}$ platelets (Figure 6A). Because it is likely that Fyn phosphorylates Tyr747 through direct interaction with the β3 cytoplasmic tail (9, 20, 31), we examined the extent to which Lnk deficiency affected (a) the association of Fyn with β3 and (b) the phosphorylation status of Tyr747 in plate-

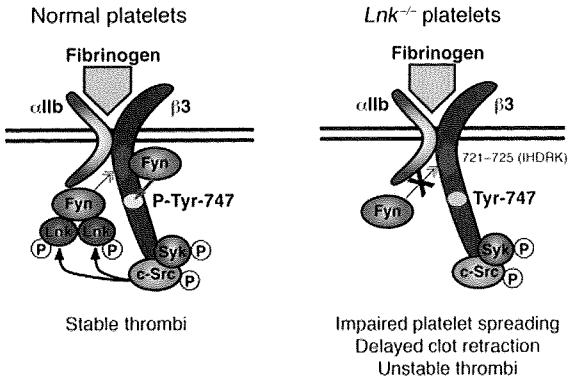

Figure 7
Model for outside-in signaling through αIIbβ3, c-Src, Fyn, and Lnk. Based on the present study, we propose that when activated, αIIbβ3 binds to fibrinogen, and a pool of c-Src constitutively bound to the cytoplasmic domain of the integrin β3 subunit initiates outside-in αIIbβ3 integrin signaling, which includes phosphorylation of Syk and its recruitment to αIIbβ3 independent of Lnk (5). The activated c-Src phosphorylates Tyr536 in a C-terminal portion of Lnk, where Lnk forms a dimeric or multimeric structure via the N-terminal domain (34). Lnk strongly facilitates Fyn recruitment to its binding site, residues 721–725 (IHDRK) in the β3 integrin tail, which may lead to phosphorylation of Tyr747 (P-Tyr747) within the β3 cytoplasmic domain of integrin αIIbβ3. Thereafter, phosphorylation of Tyr747 may facilitate thrombus stabilization in vitro and in vivo through a platelet contraction mechanism (7, 9, 40).

lets. We found that in WT platelets, Fyn co-immunoprecipitated with phosphorylated β3 and that this response was dependent upon fibrinogen ligation (Figure 6A, IP: Fyn). Furthermore, Fyn was bound to αIIbβ3 complexes immunoprecipitated 0 and 45 minutes after fibrinogen binding (Figure 6A, IP: αIIb, lanes BSA and Fbg, respectively), but this interaction was markedly diminished in *Lnk*$^{-/-}$ platelets at the same time point. The association of Fyn with Fyb was augmented by fibrinogen binding independently of Lnk (Figure 6A, IP: Fyn), and the activation of c-Src bound to αIIbβ3 (assessed based on phosphorylation of Tyr418) was comparable (Figure 6A, IP: αIIb). That Fyn is constitutively associated with the β3 integrin subunit (20) suggests that Lnk contributes to the maintenance or strength of Fyn binding to the αIIbβ3-based signaling complex without affecting c-Src activation.

Finally, we assessed the effect of Fyn deficiency on tyrosine phosphorylation of the β3 subunit and the morphology of platelets spread on fibrinogen. *Fyn*$^{-/-}$ platelets showed reduced phosphorylation of at least Tyr747 when bound to fibrinogen for 15 or 45 minutes (shown at 45 minutes, Figure 6B). In addition, in the absence of an agonist, *Fyn*$^{-/-}$ platelets exhibited delayed and impaired spreading and somewhat reduced formation of lamellipodia on fibrinogen, even after 45 minutes (Figure 6C). *Fyn*$^{-/-}$ platelets began spreading at about 20 minutes, by which time the spreading of WT platelets had already reached a plateau (data not shown). These results are consistent with the idea that Lnk sustains Fyn kinase activation of αIIbβ3, thereby regulating tyrosine phosphorylation of the β3 subunit.

Fyn-deficient mice exhibit a defect in thrombus formation similar to that seen in Lnk-deficient mice. To further examine the role of Fyn during thrombus formation in vivo, we assessed thrombus formation within mesenteric capillaries and arteries as we did for Lnk in the experiments shown in Figure 3, C and D. We found that *Fyn*$^{-/-}$ mice exhibited impaired thrombus formation that was very similar to that seen in *Lnk*$^{-/-}$ mice (Supplemental Figure 6 and Supplemental Videos 7 and 8). They also showed increased re-bleeding, but not prolonged initial bleeding times (data not shown), which is consistent with the results of Reddy et al. (20). Thus, Lnk and Fyn may act in concert to regulate αIIbβ3-based actin cytoskeletal reorganization leading to thrombus stabilization.

Discussion

Lnk is known to be a negative modulator of cytokine/growth factor receptor–mediated signaling (22) and to, perhaps, influence the motility of HSCs and progenitor cells, including their homing to (or lodging within) niches within the BM (16, 34). In addition, the proven importance of integrins and actin reorganization in HSC migration and homing (34, 35) and in megakaryocyte function (19) raises the possibility that Lnk modulates integrin signaling, but this idea has yet to be tested. In this report, we revealed a formerly unrecognized mechanism by which Lnk adaptor protein regulates integrin signaling in platelets and stabilizes developing thrombi in vivo. Using an in vivo $FeCl_3$-induced vessel occlusion model and direct imaging of platelet behavior, we showed that Lnk deficiency in platelets impairs stabilization of the developing thrombus under flow conditions, which may lead to an increase in re-bleeding events in *Lnk*$^{-/-}$ (Figure 1C) and Lnk-chimeric (Supplemental Figure 2, right) mice. Through these mechanistic studies, we have been able to demonstrate that Lnk is required for platelets to fully spread on fibrinogen (Figure 4 and Supplemental Figure 3), for efficient fibrin clot retraction (Figure 4C), for platelet aggregation in the presence of lower concentrations of an agonist (Figure 4D), and for thrombus stability under flow conditions in vivo (Figures 2 and 3). Furthermore, the findings show that all of these effects of Lnk are mediated largely by αIIbβ3-dependent outside-in signaling, which is likely associated with tyrosine phosphorylation of the β3 integrin subunit (8) or Fyn tyrosine kinase (20). We also found that ligand binding to αIIbβ3 in platelets induces the formation of a protein complex that includes αIIbβ3, c-Src, Fyn, Fyb, and Lnk (Figure 5). Formation of this complex required Src kinase activity, which targeted the C-terminal portion of Lnk (Supplemental Figure 5). Finally, we showed that Lnk supports activation of Fyn within the αIIbβ3 complex, that Fyn in turn tyrosine phosphorylates the β3 subunit (Figure 6), and that the consequences of Lnk deficiency are mirrored by Fyn deficiency (Supplemental Figure 6). In contrast to the previously described constitutive association of c-Src or Fyn with β3 (4, 31), our results indicate that the efficient binding of Fyn, but not c-Src, to the αIIbβ3 complex requires the presence of Lnk (Figure 6). When situated in close proximity to αIIbβ3, Fyn may function as a positive regulator of β3 tyrosine phosphorylation (Figure 6B) (10, 28), which would contribute to the stabilization of the thrombus (Supplemental Figure 6) (9, 20), perhaps through association of Fyn with EphA4 (7) or Bcl-3 (36). Lnk thus appears to play a previously unappreciated role in facilitating integrin αIIbβ3 outside-in signaling by acting in concert with Fyn to phosphorylate the β3 subunit on Tyr747, thereby optimizing platelet cytoskeletal reorganization for stabilization of thrombi in vivo. We therefore conclude that Lnk may selectively promote Fyn kinase regulation of αIIbβ3 outside-in signaling in platelets.

One limitation of comparing thrombus formation in Lnk- and WT-chimeras is the need to compare platelets in mice of differ-

ent ages due to the higher capacity for megakaryopoiesis in *Lnk*$^{-/-}$ animals after BM transplantation. However, using intravital microscopy after laser-induced injury, we were able to compare thrombus formation in *Lnk*$^{-/-}$ and WT mice of the same age and show that thrombus formation is impaired in *Lnk*$^{-/-}$ animals despite higher numbers of circulating platelets (Figure 3, C and D). The reduced thrombus formation by Lnk-deficient platelets was even apparent 4 weeks after transplantation, at which time chimeric mice show slight thrombocytopenia, reflecting the fact that they are recovering from severe myelosuppression, and so are actively generating platelets. Furthermore, our in vitro study of the spreading of platelets from chimeric mice of different ages confirmed that the area of spread of platelets from Lnk-chimeras was consistently smaller than the area of spread of platelets from WT-chimeras. From these findings, we again conclude that Lnk deficiency leads to impaired platelet spreading independent of age or active megakaryopoiesis and contributes to the impaired stabilization of developing thrombi in vivo.

The small GTPase Rac1 and its guanosine exchange factor Vav contribute to the formation of lamellipodia during the adhesion of CHO-αIIbβ3 cells to fibrinogen (29, 37). The activation of Rac1 is mediated through 2 NxxY motifs (residues 744–747 and 756–759 in the β3 subunit) in the cytoplasmic tail of the β3 subunit (37). Reddy et al. recently demonstrated that CHO cells expressing a truncated form of αIIbβ3 lacking the distal NxxY motif (residues 756–759) fail to spread on fibrinogen, and the defect is rescued by overexpression of active Fyn (20). Those results indicate that Fyn activation may augment functions of the proximal NxxY motif (residues 744–747), presumably through phosphorylation of Tyr747 (8). Our results support that idea and indicate that Fyn, with the help of Lnk, is required for Tyr747 phosphorylation of β3 (Figure 6, A and B). In the model cell system, Lnk was directly tyrosine phosphorylated at Tyr536 by c-Src, which was required for formation of lamellipodia by CHO-αIIbβ3 cells immobilized on fibrinogen (Supplemental Figure 5). Because Lnk supports Fyn's association with the αIIbβ3 complex but is not required for c-Src activation or its association with the αIIbβ3 complex in platelets (Figure 6A), we propose the signaling cascade depicted in Figure 7. The Fyn binding region of β3 — residues 721–725 (IHDRK) (20) — is distinct from the c-Src binding region — residues 760–762 (RGT) (38). In normal platelets, the engagement of integrin αIIbβ3 initiates outside-in signaling through c-Src activation and Syk recruitment to the β3 tail (4, 5, 31), which is independent of Lnk. The activated c-Src presumably mediates tyrosine phosphorylation of Lnk, which leads to efficient recruitment/activation of Fyn at the β3 tail and phosphorylation of Tyr747 (Figure 7). We studied the effects of CVX on inside-out signaling by measuring fibrinogen binding to integrin αIIbβ3 and on outside-in signaling by studying platelet spreading on a collagen-coated surface (data not shown). The results so far indicate that Lnk is not involved in signaling mediated through GPVI, where Fyn also functions, and it appears that Lnk deficiency does not universally affect Fyn-coupled platelet receptors. Although the precise molecular mechanism is currently unknown, presumably the necessary machinery exists to ensure the specific and selective interaction of Lnk and the Fyn complex with the β3 integrin subunit.

It has been reported that the laser-induced injury model mainly reflects the tissue factor/thrombin–mediated pathway to platelet activation and is independent of the exposed collagen-GPVI and vWF-GPIbα interactions triggered by the loss of endothelium; conversely, $FeCl_3$-induced thrombus formation is collagen and vWF dependent (23, 25, 39). Nonetheless, it is reasonable to consider that our laser-induced injury model caused relatively mild damage to endothelial cells, as compared with previously reported experimental models (26). Consistent with that idea, we found that staining of the vasculature for *Griffonia simplicifolia* IB_4 isolectin showed the endothelial layer to be intact after laser-induced injury (Supplemental Figure 7). In addition, there was no extravasation of fluorescent dyes after laser injury, indicating that vascular permeability was unaffected by laser-induced injury (Supplemental Videos 1–8). Although, as with other methods, the precise mechanism and trigger of laser-induced thrombus formation remain unclear, it is unlikely that exposure of the extracellular matrix (mainly collagen) as a result of endothelial damage is a primary trigger. One alternative possibility is that thrombus formation is triggered by ROS, but ROS produced within the blood as a result of laser irradiation of hematoporphyrin and fluorescent dyes are readily washed away by the rapid blood flow. More likely, ROS produced within endothelial cells and/or stromal spaces are involved.

Given the mild damage to the endothelium and the lack of involvement of the collagen-GPVI and vWF-GPIbα interactions, the diminished thrombus formation seen in *Lnk*$^{-/-}$ platelets could reflect a defect in αIIbβ3-mediated signaling. Recently, 2 distinct phases in the stabilization of the primary hemostatic plug under flow conditions have been proposed. The first is a rapid phase linked to fibrin-independent platelet contractility (40), possibly accomplished through αIIbβ3-mediated outside-in signaling and the subsequent Rho kinase–dependent physical tightening of platelet-platelet adhesion contacts, for example, through ephrin/Eph kinases, JAM-A, or Sema4D (41). The second is a slower phase linked to thrombin generation and fibrin polymerization to stabilize the thrombus (40).

With our imaging system and laser-induced injury, we were able to observe the rapid phase of thrombus formation, which occurs within seconds, whereas $FeCl_3$-induced arterial occlusion occurs more than 20 minutes after injury. Using chimeric mice in which platelet counts were equalized, we observed that in vivo thrombus formation by *Lnk*$^{-/-}$ platelets was impaired in both models, although more significant deficiencies were detected in the laser-injury model (Figure 2C and Figure 3A).

Recent genome-wide association studies identified SNPs associated with type 1 diabetes and celiac disease, including a nonsynonymous SNP in exon 3 of LNK/SH2B3, encoding a pleckstrin homology domain (R262W) (42, 43). Notably, the same SNP was recently shown to be associated with increased eosinophil numbers and myocardial infarction (42, 43). Accordingly, it will be important to investigate the link between the sequence variation in LNK/SH2B3 and platelet function in patients.

In conclusion, we explored a new regulatory mechanism by which the adaptor protein Lnk contributes to the stabilization of developing thrombi. Lnk regulates integrin αIIbβ3–mediated signaling in platelets and is required for Fyn interaction with αIIbβ3 and efficient tyrosine phosphorylation of the β3 integrin subunit, leading to actin cytoskeletal reorganization. Because *Lnk*$^{-/-}$ mice do not exhibit spontaneous (or abnormal) bleeding or severe immune system dysfunction, we suggest that molecules that modulate outside-in signaling, including Lnk, might represent novel and safe therapeutic targets for the prevention of cardiovascular events. Such therapeutics would likely pose a smaller risk for bleeding than conventional drugs.

Methods

Cells, reagents, and mice. All reagents were from Sigma-Aldrich unless otherwise indicated. C57BL/6 mice congenic for the Ly5 locus (B6-Ly5.1) and *Lnk*$^{-/-}$ B6-Ly5.1 mice (22) were bred and maintained at the Animal Research Centers of the Institute of Medical Science, the University of Tokyo, and of the Research Institute, International Medical Center of Japan. *Lnk*$^{-/-}$ B6-Ly5.1 mice were first established on a C57BL/6 (B6-Ly5.2) background and backcrossed more than 12 times, after which they were crossed into the B6-Ly5.1 background. WT B6-Ly5.2 mice were purchased from Nihon SLC. *Fyn*$^{-/-}$ B6-Ly5.2 mice (44) were from T. Yamamoto (University of Tokyo). The protocol for this work was approved by the IACUCs of the Institute of Medical Science, University of Tokyo, and of the Research Institute, International Medical Center of Japan. The following Abs and reagents were used: anti-c-Src (327, a gift from J. Brugge, Harvard Medical School, Boston, Massachusetts, USA) (4, 31), anti-mouse αIIbβ3 (1B5, from B. Coller, Rockefeller University, New York, New York, USA), anti-human Lnk (from J. Hayashi, University of Maryland, Baltimore, Maryland, USA, or purchased from Abcam), anti-mouse Lnk (11), anti-Lcp2 and anti-Fyb (from G. Koretzky, University of Pennsylvania, Philadelphia, USA), anti-phospho-Src pY418 and anti-phospho-β3 pY773 (Y747 in mice) (Biosource International), anti-Syk (N-19), anti-Fyn (FYN3) and anti-β3 integrin (N-20) (Santa Cruz Biotechnology Inc.), anti-phosphotyrosine (4G10) and anti-Src (GD11) (Upstate Biochemical), anti-Fyb and anti-αIIb (MWReg30, BD Biosciences and Invitrogen), HRP-conjugated secondary Abs (Bio-Rad), Protein G Sepharose (GE Healthcare), protease inhibitor cocktail, aprotinin, and leupeptin (Roche Molecular Biochemicals), rhodamine-phalloidin, Alexa Fluor 488–conjugated fibrinogen, and Alexa Fluor 488–conjugated bovine IgG Abs (Molecular Probes, Invitrogen), purified human fibrinogen (American Diagnostica Inc), FITC-conjugated anti-mouse integrin α2, αIIb, and β3 and the FITC-Annexin-V kit (BD and Invitrogen), PE–anti-mouse GPIbα, FITC–anti-mouse GPVI, and PE–anti-mouse P-selectin (Emfret), and CVX (from T. Morita, Meiji Pharmaceutical University, Tokyo, Japan).

BM transplantation. BM from femurs was washed with PBS and counted. WT (10^7 per recipient mouse) or *Lnk*$^{-/-}$ (2×10^5 or 5×10^5) BM cells were intravenously transfused into 8-week-old male Ly-5.2 recipient mice. The recipients were then lethally irradiated at a dose of 9.5 Gy. Two, 4, 6, and 8 weeks later, PBLs were collected from the recipient mice, and chimerism was confirmed using a Ly5.1/Ly5.2 system.

Bleeding times. Tail bleeding assays were performed with 8- to 12-week-old *Lnk*$^{-/-}$ and WT male mice. Mice were anesthetized with 50 μg/ml pentobarbital, after which a 5-mm segment of the distal tip of the tail was cut off, and the tail was immediately immersed in PBS at 37°C. Tail bleeding times were defined as the time required for the bleeding to stop. Tail bleeding was monitored for at least an additional 60 seconds to detect possible re-bleeding (secondary bleeding), as previously described (8, 20, 45). We preliminarily confirmed that tail bleeding and re-bleeding times were comparable in B6-Ly5.1 and B6-Ly5.2 mice.

Measurement of $FeCl_3$-induced vessel occlusion times in carotid arteries. Mice were anesthetized by injection with urethane (1.5 g/kg), and a segment of the carotid artery was exposed. Thrombus formation was then triggered by applying 10% $FeCl_3$ solution to the adventitial side to induce endothelial cell injury (23). FITC-dextran solution (5 mg/kg BW, MW 150,000) was injected via the tail vein, and carotid blood flow was continuously monitored using fluorescence confocal microscopy to determine the time to occlusion.

Intravital microscopy and thrombus formation. To visually analyze thrombus formation in the microcirculation of the mesentery in living animals, we used in vivo laser injury and visualization techniques developed through modification of conventional methods (18, 24). Male mice were anesthetized by injection with urethane (1.5 g/kg), and a small incision was made so that the mesentery could be observed without being exteriorized. FITC-dextran (5 mg/kg BW) was injected into mice to visualize cell dynamics, while hematoporphyrin (1.8 mg/kg for capillary thrombi, 2.5 mg/kg for arterioles) was injected to produce ROS upon laser irradiation. Blood cell dynamics and production of thrombi were visualized during laser excitation (λ 488 nm, 30 mW power). Sequential images were obtained for 20 seconds at 30 frames/s using a spinning-disk confocal microscope (CSU22, Yokogawa Electronics) and an EM-CCD camera (Impactron CCD; Nihon TI). The diameters of the examined capillaries were as follows: in Figure 3A, WT-chimera 6.56 ± 0.12 μm, Lnk-chimera 6.68 ± 0.06 μm (n = 30 vessels from 5 animals, P = 0.42); in Figure 3C, *Lnk*$^{-/-}$ 6.56 ± 0.12 μm, WT 6.46 ± 0.10 μm, *Lnk*$^{-/-}$ 6.56 ± 0.12 μm (n = 30 vessels from 5 animals, P = 0.26). In Figure 3D, diameters of the examined arterioles were as follows: WT 26.6 ± 4.5 μm, *Lnk*$^{-/-}$ 25.7 ± 3.4 μm (n = 10 vessels from 5 animals, P = 0.43). We also confirmed that thrombus formation within the vessels was comparable in the B6-Ly5.1 and B6-Ly5.2 mice.

Preparation of blood samples for analysis of platelet spreading and fibrinogen binding. For each experiment, blood samples were collected from 8–10 *Lnk*$^{-/-}$ and WT male mice (8–12 weeks old) by cardiac puncture after CO_2 treatment. Some collected samples were immediately transferred to plastic tubes containing one-sixth volume of acid-citrate-dextrose (ACD). Platelet-rich plasma (PRP) was obtained by centrifugation of whole blood at 150 *g* for 15 minutes without braking. To obtain the washed platelets used for most of the in vitro experiments, 1 μM PGE_1 and 2 U/ml apyrase were added, and the platelets were centrifuged at 750 *g* for 10 minutes. The sedimented platelets were then washed in modified Tyrode-HEPES buffer containing 1 μM PGE_1 plus 15% volume ACD and finally resuspended in an appropriate volume of Ca^{2+}-free modified Tyrode-HEPES buffer (10 mM HEPES [pH 7.4], 12 mM $NaHCO_3$, 138 mM NaCl, 5.5 mM glucose, 2.9 mM KCl, and 1 mM $MgCl_2$).

Confocal microscopic analysis of platelet spreading and immunoprecipitation assays. All confocal studies were performed using a Leica TCS SP2 microscope equipped with a 63×, 1.40 NA oil immersion objective (Leica), as described previously (46). Images were assembled using Adobe Photoshop. Analysis of platelet adhesion (cell number) and calculation of their surface area (spreading) were done using NIH ImageJ software (http://rsbweb.nih.gov/ij/).

The lysis buffer used for immunoprecipitation contained 2% Triton X-100 or 1% NP-40, 150 mM NaCl, 50 mM Tris-HCl (pH 7.4), 0.5 mM EGTA, 0.5 mM EDTA, 1 mM Na_3VO_4, 0.5 mM NaF, 0.5 mM PMSF, and 50 μg/ml leupeptin. Anti-αIIb was used for immunoprecipitation of αIIbβ3.

Flow cytometric measurement of fibrinogen-binding (activation of αIIbβ3) and P-selectin expression. Washed, rested platelets were incubated for 30 minutes at room temperature with 200 μg/ml Alexa Fluor 488–conjugated fibrinogen plus ADP, epinephrine, PAR4 agonist peptide, or PMA in a 50-μl final volume of modified Tyrode-HEPES buffer containing 0.2 mM $CaCl_2$. The binding of Alexa Flour 488–fibrinogen to platelets was quantified using an Aria flow cytometer (BD). Nonspecific binding was determined in the presence of 20 μg/ml 1B5. Specific binding was defined as total minus the nonspecific binding. P-selectin expression was measured similarly using a Canto-II flow cytometer (BD) with washed platelets in a 100-μl final volume (1×10^6 platelets).

Clot retraction assay. To obtain washed platelets, PRP from WT or *Lnk*$^{-/-}$ mice was diluted with 1 volume of modified Tyrode-HEPES buffer and centrifuged in the presence of 0.15 μM PGE_1. The sedimented platelets were then washed in modified Tyrode-HEPES buffer containing 0.15 μM PGE_1 and 1 mM EDTA and finally resuspended with modified Tyrode-HEPES buffer to adjust the number of platelets to 3×10^8/ml. Fibrin clot retraction was studied by incubating the clots in the presence of 2 U/ml

thrombin, 500 μg/ml fibrinogen, and 2 mM $CaCl_2$ for 1 or 2 hours at 37°C in an aggregometer cuvette as described previously (47, 48).

Plasmids and transfection of COS7 or CHO cells. COS7 and CHO-αIIbβ3 cells (provided by H. Kashiwagi, Osaka University, Osaka, Japan) were transfected using Lipofectamine 2000 methodology (Invitrogen). Constitutively active human c-Src mutant (Y530F)/pcDNA3 was obtained from T. Tezuka (University of Tokyo). Flag-tagged Lnk and the C-terminal deletion mutant (ΔC-Lnk) were constructed by PCR using previously constructed plasmids (34) as templates and reinserted into pcDNA3 vector. A Lnk cDNA cassette lacking the stop codon was generated by PCR and inserted into pcDNA-DEST47 (Invitrogen) to generate the expression vector for the Lnk-GFP fusion protein, as described previously (34).

Statistics. Differences between experimental and control animals were analyzed using 2-tailed Student's *t* tests. Incidence of re-bleeding times was evaluated by the χ^2 test. *P* values less than 0.05 were considered significant.

Acknowledgments

The authors thank J. Brugge, B. Coller, J. Hayashi, H. Kashiwagi, G. Koretzky, T. Morita, and T. Tezuka for providing reagents or cells and T. Yamamoto for *Fyn*-null mice. We are also grateful to J. Seita, H. Tsukui, A. Yamasaki, K. Wakabayashi, and M. Tajima for their excellent technical help. This work was supported by Grants-in-Aid and Special Coordination Funds for Promoting Science and Technology from the Ministry of Education, Culture, Sports, Science and Technology and from the Ministry of Health, Labour and Welfare, by the Japanese Sharyou Foundation (Tokyo, Japan), by the Uehara Memorial Foundation (Tokyo, Japan), and by the Mitsubishi Pharma Research Foundation (Osaka, Japan). H. Takizawa and S. Nishimura are supported by a fellowship for Japanese Junior Scientists from the Japan Society for the Promotion of Science.

Received for publication April 9, 2009, and accepted in revised form October 28, 2009.

Address correspondence to: Koji Eto, Division of Stem Cell Bank, The Institute of Medical Science, The University of Tokyo, 4-6-1 Shirokanedai, Minato-ku, Tokyo, 108-8639 Japan. Phone: 81-3-6409-2342; Fax: 81-3-6409-2343; E-mail: keto@ims.u-tokyo.ac.jp. Or to: Satoshi Takaki, Research Institute, International Medical Center of Japan, 1-21-1 Toyama, Shinjuku-ku, Tokyo, 162-8655 Japan. Phone: 81-3-3202-7181; Fax: 81-3-3208-5421; E-mail: stakaki@ri.imcj.go.jp.

1. Shattil SJ, Newman PJ. Integrins: dynamic scaffolds for adhesion and signaling in platelets. *Blood.* 2004;104(6):1606–1615.
2. Ruggeri ZM. Platelets in atherothrombosis. *Nat Med.* 2002;8(11):1227–1234.
3. Inoue O, et al. Laminin stimulates spreading of platelets through integrin alpha6beta1-dependent activation of GPVI. *Blood.* 2006;107(4):1405–1412.
4. Obergfell A, et al. Coordinate interactions of Csk, Src, and Syk kinases with [alpha]IIb[beta]3 initiate integrin signaling to the cytoskeleton. *J Cell Biol.* 2002;157(2):265–275.
5. Shattil SJ. Integrins and Src: dynamic duo of adhesion signaling. *Trends Cell Biol.* 2005;15(8):399–403.
6. Arias-Salgado EG, et al. PTP-1B is an essential positive regulator of platelet integrin signaling. *J Cell Biol.* 2005;170(5):837–845.
7. Prevost N, et al. Eph kinases and ephrins support thrombus growth and stability by regulating integrin outside-in signaling in platelets. *Proc Natl Acad Sci U S A.* 2005;102(28):9820–9825.
8. Law DA, et al. Integrin cytoplasmic tyrosine motif is required for outside-in alphaIIbbeta3 signalling and platelet function. *Nature.* 1999;401(6755):808–811.
9. Phillips DR, Nannizzi-Alaimo L, Prasad KS. Beta3 tyrosine phosphorylation in alphaIIbbeta3 (platelet membrane GP IIb-IIIa) outside-in integrin signaling. *Thromb Haemost.* 2001;86(1):246–258.
10. Xi X, et al. Tyrosine phosphorylation of the integrin beta 3 subunit regulates beta 3 cleavage by calpain. *J Biol Chem.* 2006;281(40):29426–29430.
11. Takaki S, et al. Control of B cell production by the adaptor protein lnk. Definition of a conserved family of signal-modulating proteins. *Immunity.* 2000;13(5):599–609.
12. Takaki S, Morita H, Tezuka Y, Takatsu K. Enhanced hematopoiesis by hematopoietic progenitor cells lacking intracellular adaptor protein, Lnk. *J Exp Med.* 2002;195(2):151–160.
13. Velazquez L, et al. Cytokine signaling and hematopoietic homeostasis are disrupted in Lnk-deficient mice. *J Exp Med.* 2002;195(12):1599–1611.
14. Tong W, Lodish HF. Lnk inhibits Tpo-mpl signaling and Tpo-mediated megakaryocytopoiesis. *J Exp Med.* 2004;200(5):569–580.
15. Tong W, Zhang J, Lodish HF. Lnk inhibits erythropoiesis and Epo-dependent JAK2 activation and downstream signaling pathways. *Blood.* 2005;105(12):4604–4612.
16. Buza-Vidas N, et al. Cytokines regulate postnatal hematopoietic stem cell expansion: opposing roles of thrombopoietin and LNK. *Genes Dev.* 2006;20(15):2018–2023.
17. Seita J, et al. Lnk negatively regulates self-renewal of hematopoietic stem cells by modifying thrombopoietin-mediated signal transduction. *Proc Natl Acad Sci U S A.* 2007;104(7):2349–2354.
18. Falati S, Gross P, Merrill-Skoloff G, Furie BC, Furie B. Real-time in vivo imaging of platelets, tissue factor and fibrin during arterial thrombus formation in the mouse. *Nat Med.* 2002;8(10):1175–1181.
19. Takizawa H, et al. Growth and maturation of megakaryocytes is regulated by Lnk/Sh2b3 adaptor protein through crosstalk between cytokine- and integrin-mediated signals. *Exp Hematol.* 2008;36(7):897–906.
20. Reddy KB, Smith DM, Plow EF. Analysis of Fyn function in hemostasis and alphaIIbbeta3-integrin signaling. *J Cell Sci.* 2008;121(Pt 10):1641–1648.
21. Fitau J, Boulday G, Coulon F, Quillard T, Charreau B. The adaptor molecule Lnk negatively regulates tumor necrosis factor-alpha–dependent VCAM-1 expression in endothelial cells through inhibition of the ERK1 and -2 pathways. *J Biol Chem.* 2006;281(29):20148–20159.
22. Ema H, et al. Quantification of self-renewal capacity in single hematopoietic stem cells from normal and Lnk-deficient mice. *Dev Cell.* 2005;8(6):907–914.
23. Dubois C, Panicot-Dubois L, Merrill-Skoloff G, Furie B, Furie BC. Glycoprotein VI-dependent and -independent pathways of thrombus formation in vivo. *Blood.* 2006;107(10):3902–3906.
24. Nishimura S, et al. In vivo imaging in mice reveals local cell dynamics and inflammation in obese adipose tissue. *J Clin Invest.* 2008;118(2):710–721.
25. Dubois C, Panicot-Dubois L, Gainor JF, Furie BC, Furie B. Thrombin-initiated platelet activation in vivo is vWF independent during thrombus formation in a laser injury model. *J Clin Invest.* 2007;117(4):953–960.
26. Furie B, Furie BC. In vivo thrombus formation. *J Thromb Haemost.* 2007;5(Suppl 1):12–17.
27. Juliano RL, Redding P, Alahari S, Edin M, Howe A, Aplin A. Integrin regulation of cell signaling and motility. *Biochem Soc Trans.* 2004;32(pt 3):443–446.
28. Blystone SD. Kinetic regulation of beta 3 integrin tyrosine phosphorylation. *J Biol Chem.* 2002;277(49):46886–46890.
29. Obergfell A, et al. The molecular adapter SLP-76 relays signals from platelet integrin alphaIIbbeta3 to the actin cytoskeleton. *J Biol Chem.* 2001;276(8):5916–5923.
30. Jordan MS, Singer AL, Koretzky GA. Adaptors as central mediators of signal transduction in immune cells. *Nat Immunol.* 2003;4(2):110–116.
31. Arias-Salgado EG, et al. Src kinase activation by direct interaction with the integrin beta cytoplasmic domain. *Proc Natl Acad Sci U S A.* 2003; 100(23):13298–13302.
32. Salsmann A, Schaffner-Reckinger E, Kabile F, Plancon S, Kieffer N. A new functional role of the fibrinogen RGD motif as the molecular switch that selectively triggers integrin alphaIIbbeta3-dependent RhoA activation during cell spreading. *J Biol Chem.* 2005;280(39):33610–33619.
33. Petrich BG, et al. The antithrombotic potential of selective blockade of talin-dependent integrin alpha IIb beta 3 (platelet GPIIb-IIIa) activation. *J Clin Invest.* 2007;117(8):2250–2259.
34. Takizawa H, et al. Enhanced engraftment of hematopoietic stem/progenitor cells by the transient inhibition of an adaptor protein, Lnk. *Blood.* 2006;107(7):2968–2975.
35. Cancelas JA, et al. Rac GTPases differentially integrate signals regulating hematopoietic stem cell localization. *Nat Med.* 2005;11(8):886–891.
36. Weyrich AS, et al. Signal-dependent translation of a regulatory protein, Bcl-3, in activated human platelets. *Proc Natl Acad Sci U S A.* 1998; 95(10):5556–5561.
37. Berrier AL, Martinez R, Bokoch GM, LaFlamme SE. The integrin beta tail is required and sufficient to regulate adhesion signaling to Rac1. *J Cell Sci.* 2002;115(Pt 22):4285–4291.
38. Arias-Salgado EG, Lizano S, Shattil SJ, Ginsberg MH. Specification of the direction of adhesive signaling by the integrin beta cytoplasmic domain. *J Biol Chem.* 2005;280(33):29699–29707.
39. Izuhara Y, et al. Inhibition of plasminogen activator inhibitor-1: its mechanism and effectiveness on coagulation and fibrosis. *Arterioscler Thromb Vasc Biol.* 2008;28(4):672–677.
40. Ono A, et al. Identification of a fibrin-independent platelet contractile mechanism regulating primary hemostasis and thrombus growth. *Blood.* 2008;112(1):90–99.
41. Brass LF, Zhu L, Stalker TJ. Novel therapeutic targets at the platelet vascular interface. *Arterioscler Thromb Vasc Biol.* 2008;28(3):s43–s50.
42. Hunt KA, et al. Newly identified genetic risk vari-

ants for celiac disease related to the immune response. *Nat Genet.* 2008;40(4):395–402.
43. Gudbjartsson DF, et al. Sequence variants affecting eosinophil numbers associate with asthma and myocardial infarction. *Nat Genet.* 2009;41(3):342–347.
44. Yagi T, et al. Regional localization of Fyn in adult brain; studies with mice in which fyn gene was replaced by lacZ. *Oncogene.* 1993;8(12):3343–3351.
45. Kasirer-Friede A, et al. ADAP is required for normal alphaIIbbeta3 activation by VWF/GP Ib-IX-V and other agonists. *Blood.* 2007;109(3):1018–1025.
46. Eto K, et al. The WAVE2/Abi1 complex differentially regulates megakaryocyte development and spreading: implications for platelet biogenesis and spreading machinery. *Blood.* 2007;110(10):3637–3647.
47. Prevost N, Kato H, Bodin L, Shattil SJ. Platelet integrin adhesive functions and signaling. *Methods Enzymol.* 2007;426:103–115.
48. Suzuki-Inoue K, et al. Involvement of Src kinases and PLCgamma2 in clot retraction. *Thromb Res.* 2007;120(2):251–258.

TGF-β as a candidate bone marrow niche signal to induce hematopoietic stem cell hibernation

Satoshi Yamazaki,[1,2] Atsushi Iwama,[3,4] Shin-ichiro Takayanagi,[1] Koji Eto,[1] Hideo Ema,[1] and Hiromitsu Nakauchi[1,5]

[1]Laboratory of Stem Cell Therapy, Center for Experimental Medicine, The Institute of Medical Science, University of Tokyo, Tokyo; [2]ReproCELL, Tokyo; [3]Department of Cellular and Molecular Medicine, Graduate School of Medicine, Chiba University, Chiba; and [4]Japan Science and Technology Agency (JST), Core Research for Evolutional Science and Technology (CREST) and [5]JST, Exploratory Research for Advanced Technology (ERATO), Sanbancho, Chiyoda-ku, Tokyo, Japan

Hematopoietic stem cells (HSCs) reside in a bone marrow niche in a nondividing state from which they occasionally are aroused to undergo cell division. Yet, the mechanism underlying this unique feature remains largely unknown. We have recently shown that freshly isolated CD34⁻KSL hematopoietic stem cells (HSCs) in a hibernation state exhibit inhibited lipid raft clustering. Lipid raft clustering induced by cytokines is essential for HSCs to augment cytokine signals to the level enough to re-enter the cell cycle. Here we screened candidate niche signals that inhibit lipid raft clustering, and identified that transforming growth factor-β (TGF-β) efficiently inhibits cytokine-mediated lipid raft clustering and induces HSC hibernation ex vivo. Smad2 and Smad3, the signaling molecules directly downstream from and activated by TGF-β receptors were specifically activated in CD34⁻KSL HSCs in a hibernation state, but not in cycling CD34⁺KSL progenitors. These data uncover a critical role for TGF-β as a candidate niche signal in the control of HSC hibernation and provide TGF-β as a novel tool for ex vivo modeling of the HSC niche. (Blood. 2009;113:1250-1256)

Introduction

Dormancy or hibernation of hematopoietic stem cells (HSCs), which is indispensable for HSC maintenance, is known to occur solely in the particular bone marrow (BM) microenvironment known as the HSC niche. Most of the HSCs are in the G_0 phase in the BM niche. However, HSCs are recruited into the cell cycle at long intervals, on average every 1 to 2 months.[1,2] Thus, the capacity to enter and to leave a hibernation-like state is one of the properties of "stemness." The so-called stromal cells in the HSC BM niche, including osteoblasts, fibroblasts, adipocytes, and endothelial cells, produce several secreted and membrane-bound growth factors.[3] Several signaling pathways have been characterized that keep HSCs in hibernation or undifferentiated states. These include the Ang-1–Tie-2 signal,[4] the Notch ligand–Notch signal,[5] the N-cadherin homotypic signal,[6] and the transforming growth factor-β (TGF-β) signal.[7] However, the precise molecular mechanisms underlying HSC hibernation remain largely elusive.

Mouse BM HSCs are enriched exclusively in CD34⁻c-Kit⁺ Sca-1⁺ lineage marker–negative (Lin⁻) (CD34⁻KSL) cells, a population representing 0.004% of BM mononuclear cells, whereas CD34⁺KSL cells are progenitors with short-term repopulating capacity.[8] We have recently reported that HSCs use the PI3K-Akt-FoxO signaling pathway to regulate their hibernation state, as does *C elegans* in dauer formation.[9] Akt is inactive in the cytoplasm of freshly isolated hibernating CD34⁻KSL HSCs, and FoxOs, its downstream targets, are active in their nuclei. In contrast, Akt is active in cycling CD34⁺KSL progenitors and phosphorylated FoxOs are excluded to the cytoplasm. Of note is our discovery that lipid raft status finely tunes cytokine signal levels and regulates Akt activity. Lipid raft microdomains are cholesterol- and glycosphingolipid-enriched patches in the plasma membrane into which various functional molecules are distributed. Lipid rafts act as platforms for cellular functions that include cytokine signaling, membrane trafficking, and cytoskeleton organization.[10] Because larger rafts have greater potential for concentration of transducers and for exclusion of negative regulators, lipid raft size controls signal intensity and functional outcomes. HSCs freshly isolated from the BM niche lacked lipid raft clustering (LRC). However, cytokine-induced LRC was essential for augmentation of HSC cytokine signals to levels sufficient for cell-cycle re-entry. Conversely, inhibition of LRC in HSCs attenuated cytokine signals, leading to repression of Akt followed by sustained nuclear accumulation of FoxOs, and induced a hibernation-like state in CD34⁻KSL HSCs ex vivo.

The FoxO subfamily of transcription factors is involved in diverse physiologic processes.[11] Upon activation by growth factors, the serine/threonine kinase Akt directly phosphorylates FoxO1, FoxO3, and FoxO4, resulting in their nuclear exclusion and subsequent degradation. In the absence of growth factors or in the presence of stressful stimuli, FoxOs are translocated to the nucleus and up-regulate the expression of a series of target genes, thereby promoting cell-cycle arrest, stress resistance, or apoptosis.[12] Mice that were conditionally deleted of *FoxO1, FoxO3,* and *FoxO4* in adult hematopoietic system exhibited defective long-term repopulating activity that correlated with increased cell cycling and apoptosis of HSCs.[13] Levels of reactive oxygen species (ROSs) were intriguingly increased in *FoxO*-deficient HSCs; in vivo treatment with the antioxidative agent *N*-acetyl-L-cysteine (NAC) rescued the *FoxO*-deficient HSC phenotype. Even in mice deficient

Submitted April 4, 2008; accepted July 27, 2008. Prepublished online as *Blood* First Edition paper, October 22, 2008; DOI 10.1182/blood-2008-04-146480.

An Inside *Blood* analysis of this article appears at the front of this issue.

The online version of this article contains a data supplement.

The publication costs of this article were defrayed in part by page charge payment. Therefore, and solely to indicate this fact, this article is hereby marked "advertisement" in accordance with 18 USC section 1734.

for a single *FoxO* gene, *FoxO3a,* much milder but similar defects were observed.[14] These results suggest that FoxOs play essential roles in the establishment of resistance to physiologic oxidative stress, a resistance necessary to ensure the quiescence, survival, and function of HSCs. These findings demonstrate a tight correlation between lipid raft status and Akt-FoxO signaling in the context of HSC hibernation and survival and indicate that LRC plays a key role in HSC emergence from hibernation and that LRC-inhibitory signals from the BM niche are critical in the induction and maintenance of HSC hibernation.

One of the niche signaling molecules, TGF-β, acts as a negative regulator of hematopoietic stem and progenitor cell proliferation in vitro.[7] Upon association with TGF-β, TGF-β type II receptor (TβRII) forms a complex with TGF-β type I receptor (TβRI). Subsequently, the activated TGF-β receptor complex phosphorylates receptor-activated Smads (R-Smad2) and R-Smad3. R-Smads eventually heterodimerize with the common mediator Smad4, and the resulting complex translocates to the nucleus and recruits transcriptional cofactors to control expression of genes, including those involved in the cell cycle. It has been reported that TGF-β1–null mice and inducible TβRII knockout models develop a transplantable lethal inflammatory disorder affecting multiple organs.[15,16] However, mice deficient in the TβRI, activin receptor-like kinase 5 (ALK-5), show no defects in HSC quiescence or in maintenance of the HSC pool.[17] Mice deficient for the TGF-β type II receptor have not been well characterized with respect to HSC hibernation.[16] TGF-β signaling deficiency so far has not revealed any effect on HSC proliferation and differentiation in vivo. Therefore, the outcome of TGF-β signaling is believed to be context dependent in hematopoiesis and the regulation of hematopoietic stem and progenitor cells is more complicated in the BM microenvironment in vivo than is seen in liquid cultures ex vivo.

In this study, we screened candidate niche signals that inhibit lipid raft clustering and identified that TGF-β efficiently inhibits cytokine-mediated LRC. We further characterized its role in HSC hibernation.

Methods

Mice

C57BL/6 (B6-Ly5.2) mice were purchased from Japan SLC (Shizuoka, Japan). C57BL/6 mice congenic for the Ly5 locus (B6-Ly5.1) were purchased from Sankyo-Lab Service (Tsukuba, Japan). C57BL/6 Ly5.1 × Ly5.2 F1 mice were bred and maintained in the Animal Research Facility of the Institute of Medical Science, University of Tokyo. Animal care in our laboratory was in accord with the guidance of Tokyo University for animal and recombinant DNA experiments.

Purification of mouse HSCs and CD34$^+$KSL cells

Mouse CD34$^-$KSL HSCs and CD34$^+$KSL progenitor cells were purified from BM cells of 2-month-old mice. In brief, low-density cells were isolated on Lymphoprep (1.086 g/mL; Nycomed, Oslo, Norway). The cells were stained with an antibody cocktail consisting of biotinylated anti–Gr-1, –Mac-1, –B220, -CD4, -CD8, and –Ter-119 monoclonal antibodies (PharMingen, San Diego, CA). Lineage-positive cells were depleted with antibiotin MicroBeads (Miltenyi Biotec, Bergisch Gladbach, Germany). The remaining cells were further stained with fluorescein isothiocyanate (FITC)–conjugated anti-CD34, phycoerythrin (PE)–conjugated anti–Sca-1, and allophycocyanin (APC)–conjugated anti–c-Kit antibodies (PharMingen). Biotinylated antibodies were detected with streptavidin-APC Cy7 (Molecular Probes, Eugene, OR). Analysis and cell sorting were performed on a MoFlo using Summit software (Dako, Glostrup, Denmark) and results were analyzed with FlowJo software (TreeStar, Ashland, OR).[18]

Immunofluorescent staining and linearization analysis

The markers and antibodies used were the DNA marker 4,6-diamidino-2-phenylindole (DAPI), Alexa-488–conjugated cholera toxin B subunit (CTxB), Alexa-647–conjugated goat anti–rabbit IgG, goat anti–mouse IgG, and Alexa-488–conjugated goat anti–rabbit IgG (Molecular Probes, Carlsbad, CA), rabbit anti–phospho-Akt and rabbit anti-FOXO3a (Upstate Cell Signaling, Charlottesville, VA), rabbit anti-p57 (Santa Cruz Biotechnology, Santa Cruz, CA), rabbit anti–phospho-Smad2/3 (CHEMICON, Temecula, CA), and rabbit anti–phospho-Src (Y418; Biosource, Camarillo, CA). Individual CD34$^-$ KSL cells were sorted into a serum-free culture-medium drop supplemented with 50 ng/mL mouse SCF and/or 50 ng/mL human TPO on slide glasses. The sorted cells were incubated at 37°C for the indicated time periods. After fixation with 2% paraformaldehyde and blocking in 10% goat serum for 1 hour at room temperature, cells were incubated with a primary antibody for 12 hours at 4°C. The cells were then washed and were incubated with a secondary antibody for 30 minutes at room temperature. Immunofluorescence was observed with a Leica TCS SP2 AOBS confocal microscope (Wetzlar, Germany) or with an Olympus Laser Scanning Cytometer 2 (LSC2; Tokyo, Japan).

Single-cell culture

CD34$^-$KSL cells were clonally deposited into 96-well microtiter plates containing 200 μL S-Clone SF-03 (Sanko Junyaku, Tokyo, Japan) supplemented with 5×10^{-5} M 2-β-mercaptoethanol, 10% FCS, and the indicated cytokines (20 ng/mL mouse SCF, 50 ng/mL human TPO, 20 ng/mL mouse IL-3, and 2 U/mL human EPO) in the presence or absence of 5 ng/mL human TGF-β1, TGF-β2, TGF-β3, latent TGF-β1, Activin-A, and Nodal (R&D Systems, Minneapolis, MN). Survival and cell division of HSCs were monitored by microscopy. To allow colony formation, single HSCs were cultured in the presence of SCF, TPO, IL-3, EPO, and anti–TGF-β blocking antibody (R&D Systems) for 11 days. Colonies were recovered, cytospun onto glass slides, and subjected to May-Grünwald-Giemsa staining for morphologic examination.

Competitive repopulation assays

Competitive repopulation assays were performed using the Ly5 system. In brief, single cultured HSCs or pooled single cultured HSCs (B6-Ly5.1) were mixed with 2×10^5 BM competitor cells (B6-F1) and were transplanted into B6-Ly5.2 mice irradiated at a dose of 9.5 Gy. After transplantation, peripheral blood cells of the recipients were stained with biotinylated anti-Ly5.1 (A20) and FITC-conjugated anti-Ly5.2. The cells were simultaneously stained with PE-Cy7–conjugated anti-B220 antibody, a mixture of APC-conjugated anti–Mac-1 and –Gr-1 antibodies, or a mixture of PE-conjugated anti-CD4 and -CD8 antibodies (PharMingen). Biotinylated antibody was developed with streptavidin Alexa-594 (Molecular Probes, Carlsbad, CA). The cells were analyzed on a fluorescence-activated cell sorting (FACS) Vantage (BD. Franklin Lakes, NJ). Percentage chimerism was calculated as (percentage Ly5.1 cells) × 100/(percentage Ly5.1 cells + percentage F1 cells). When percentage chimerism of donor-derived cells was more than 1.0 (summed over myeloid, B-lymphoid, and T-lymphoid lineages), recipient mice were considered to be multilineage reconstituted (positive mice).

RT-PCR

Semiquantitative RT-PCR was carried out using normalized cDNA and quantitative PCR with TaqMan rodent GAPDH control reagent (Perkin-Elmer Applied Biosystems, Foster City, CA) as previously described.[19] Cycling parameters were as follows: denaturation at 95°C for 15 seconds, annealing at 58°C for 15 seconds, and extension at 72°C for 30 seconds. Amplification proceeded for 38 cycles. PCR products were separated on 1.4% agarose gels and visualized by ethidium bromide staining.

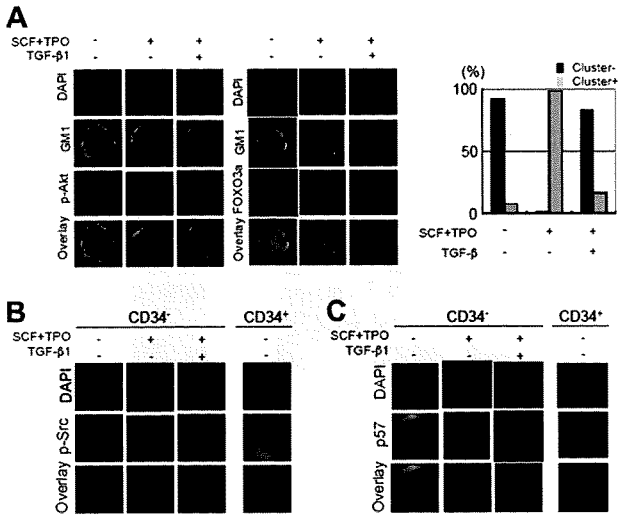

Figure 1. TGF-β inhibits LRC and attenuates cytokine signals. (A) TGF-β inhibits cytokine-mediated LRC and maintains repression of the Akt-FoxO pathway in HSCs. Freshly isolated CD34$^-$KSL HSCs were sorted into individual serum-free culture-medium drops on slide glasses. The sorted cells were incubated at 37°C for 30 minutes in the presence or absence of TGF-β1, and then were stimulated with SCF and TPO for another 30 minutes. The cells were stained with DAPI (blue), CTxB (green), and an anti–phospho-Akt (red) or an anti-FoxO3a antibody (red). Proportions of CD34$^-$KSL HSCs that showed lipid raft cluster formation are indicated as gray bars (Cluster+; right panel). (B) TGF-β inhibits activation of c-Src in HSCs. Freshly isolated CD34$^-$KSL HSCs were incubated in the presence or absence of TGF-β1 for 30 minutes and then were stimulated with SCF and TPO for another 30 minutes. Freshly isolated CD34$^+$KSL progenitor cells were also subjected to analysis. The cells were stained with DAPI (blue) and an anti–phospho-c-Src antibody (red). (C) TGF-β maintains cytoplasmic accumulation of p57 in HSCs. Freshly isolated CD34$^-$KSL HSCs were incubated in the presence or absence of TGF-β1 for 30 minutes and then were stimulated with SCF and TPO for another 30 minutes. Freshly isolated CD34$^+$KSL progenitor cells were also subjected to analysis. The cells were stained with DAPI (blue) and an anti-p57 antibody (green).

Results

TGF-β inhibits LRC and attenuates cytokine signals in HSCs

Whereas HSCs are exposed to a variety of secreted and membrane-bound growth factors in the BM,[3] lipid rafts are diffusely distributed on freshly isolated CD34$^-$KSL HSCs but are highly polarized or clustered on CD34$^+$KSL progenitor cells.[9] This suggests that LRC is tightly inhibited on HSCs in the BM niche. We hypothesized that some signals from the niche act against LRC and keep HSCs in hibernation. Several niche signals are associated with HSC dormancy. These include the Ang-1–Tie-2 signal, the Notch ligand–Notch signal, the N-cadherin homotypic signal, the TGF-β signal, and so on. We tested the effects of these signals on LRC in HSCs.

Lipid raft distribution was assessed using cholera toxin subunit B (CTxB) to label endogenous GM1 ganglioside, a component of lipid rafts. Freshly isolated CD34$^-$KSL HSCs were incubated with Ang-1, TGF-β1, or the Notch ligand Jagged-1 for 1 hour, and were then stimulated with SCF and TPO, cytokines supportive of HSC self-renewal and survival, for 30 minutes. As reported, stimulation of HSCs by cytokines induced LRC. Jagged-1 had no antagonistic effect at all on LRC. Ang-1 partially inhibited LRC, but not enough to inhibit activation of the Akt-FoxO pathway and to induce cell-cycle arrest (data not shown). In contrast, TGF-β strikingly inhibited SCF- and TPO-induced LRC (Figure 1A). TGF-β1 also inhibited Akt activation and caused sustained nuclear accumulation of FOXO3a (Figure 1A). Lipid raft protein components include transmembrane antigens/receptors, GPI-anchored proteins, cytoskeletal proteins, Src-family kinases, G-proteins, and other proteins involved in signal transduction. Treatment of HSCs with PP2, an inhibitor specific for Src-family kinases, inhibited LRC (Figure S1, available on the *Blood* website; see the Supplemental Materials link at the top of the online article). Intriguingly, TGF-β1 similarly suppressed the cytokine-mediated activation of c-Src tyrosine kinase (Figure 1B). Hibernating HSCs express high levels of cytoplasmic cyclin D1 and p57 cyclin–dependent kinase inhibitor (CDKI). Cytokine stimulation induces nuclear translocation of cyclin D1 and disappearance of p57, which is supposedly due to rapid protein degradation.[9] TGF-β1 inhibited nuclear translocation of cyclin D1 (data not shown) and kept p57 in the cytoplasm (Figure 1C). These effects of TGF-β1 on HSCs were comparable with that of β-cyclodextrin (MβCD), which inhibits LRC by depleting plasma membrane cholesterol.[9]

TGF-β induces HSC hibernation ex vivo

We then asked whether TGF-β induces quiescence in HSCs. Single CD34$^-$KSL HSCs were cultured in the presence of SCF, TPO, and TGF-β1. In the presence of SCF and TPO, more than 85% of HSCs proliferated robustly, but in the absence of SCF or TPO, none survived more than 24 hours (data not shown). In contrast, addition of TGF-β1 in culture strongly suppressed colony formation of single HSCs in a dose-dependent manner (Figure S2). Detailed observation revealed that addition of 5 ng/mL TGF-β1 in culture strongly suppressed division of single HSCs that, however, remained alive. During 5-day culture, 57% of single HSCs stayed dormant, that is, persisted as living single cells, and 22% of single HSCs divided only once (Figure 2A). Similar results were obtained when HSCs were cultured under another HSC-supporting cytokine condition, SCF plus IL-11 (Figure S3). After culture medium was changed to an optimal medium supplemented with SCF, TPO, IL-3, and EPO, 72.2% of single HSCs, which had stayed dormant for 5 days, gave rise to colonies; of these, 47% were neutrophil/macrophage/erythroblast/megakaryocyte (nmEM) colonies, derived from colony-forming units–nmEM (CFU-nmEMs) with multipotency, that is, a full range of differentiation capacity along myeloid lineages (Figure 2B). Thus, 33.9% of surviving single HSCs could retrospectively be inferred to have been CFU-nmEMs. Even after 7 days of culture, most single HSCs retained multipotency (Figure 2B). These data demonstrate that TGF-β can keep HSCs in hibernation without loss of higher-order biologic potential ex vivo. Furthermore, when we compared the activities of TGF-β1, TGF-β2, and TGF-β3 with respect to induction of the hibernating state, some HSCs survived as single cells for more than 15 days in culture in the presence of TGF-β3 (Figure S4).

To obtain direct evidence of HSC activity, we performed competitive hematopoiesis repopulation assays in vivo. We again selected single HSCs that had not divided during 5-day clonal single-cell culture in the presence of SCF, TPO, and TGF-β. Single HSCs or pools comprising 20 individual HSCs were transplanted into lethally irradiated recipient mice. As a control, freshly isolated single HSCs or pools comprising 20 individual HSCs were similarly transplanted. Comparable proportions of freshly isolated and cultured hibernating (in the presence of TGF-β) single HSCs exhibited LTR activity (26% and 20%, respectively); establishment of chimerism also was comparable (13.5% and 9.5%, respectively) (Figure 2C). In contrast, when single HSCs were cultured in the presence of SCF and TPO without TGF-β, they robustly proliferated but lost LTR activity (data not shown). All recipient mice infused with pools of 20 freshly isolated HSCs showed donor cell repopulation. So did those infused with pools of 20 cultured single

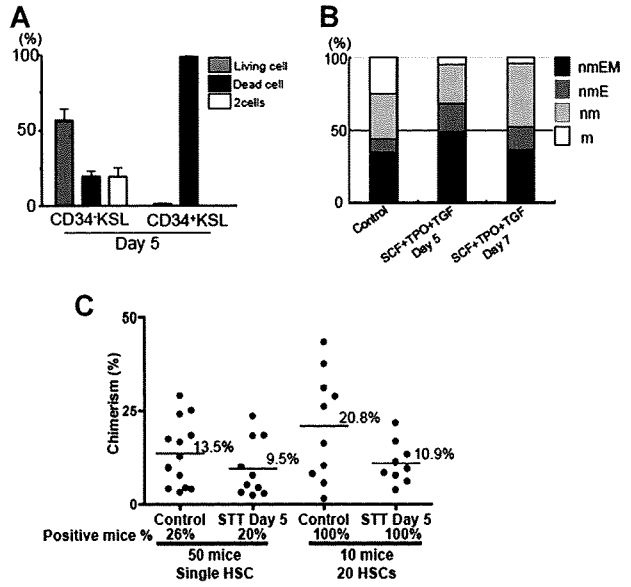

Figure 2. TGF-β induces HSC hibernation ex vivo. (A) Freshly isolated CD34⁻KSL HSCs and CD34⁺KSL hematopoietic progenitor cells were sorted clonally into 96-well microtiter plates and incubated in the presence of SCF, TPO, and TGF-β1. At day 5 of culture, cell viability and cell numbers were assessed under an inverted microscope. (B) Freshly isolated CD34⁻KSL HSCs were sorted clonally into 96-well microtiter plates and incubated in the presence of SCF, TPO, and TGF-β1. At the indicated time points, surviving single HSCs that had not divided were selected. Culture medium was replaced with one supplemented with SCF, TPO, IL-3, and EPO, permitting colony formation. After 14 subsequent days of culture, the colonies were recovered for morphologic examination. As a control, freshly isolated CD34⁻KSL HSCs were sorted clonally into 96-well microtiter plates supplemented with SCF, TPO, IL-3, and EPO and cultured for 14 days. Proportions of colony types are depicted: n indicates neutrophils; m, macrophages; E, erythroblasts; and M, megakaryocytes. (C) Freshly isolated CD34⁻KSL HSCs were sorted clonally into 96-well microtiter plates and were incubated in the presence of SCF, TPO, and TGF-β1. At day 5 of culture, surviving single HSCs that had not divided during 5-day culture were selected. Single HSCs or pools of 20 single HSCs (indicated by STT day 5; B6-Ly5.1) were mixed with B6-Ly5.2 competitor cells and injected into lethally irradiated B6-Ly5.2 recipient mice. As a control, freshly isolated single-HSC or 20-HSCs pools were similarly transplanted into recipient mice. Percentage chimerism of donor cells in recipient mice 12 weeks after transplantation is plotted as dots, with mean values indicated as bars. Recipient mice with donor cell chimerism more than 1.0% for myeloid and for B- and T-lymphoid lineages were considered multilineage reconstituted (positive mice).

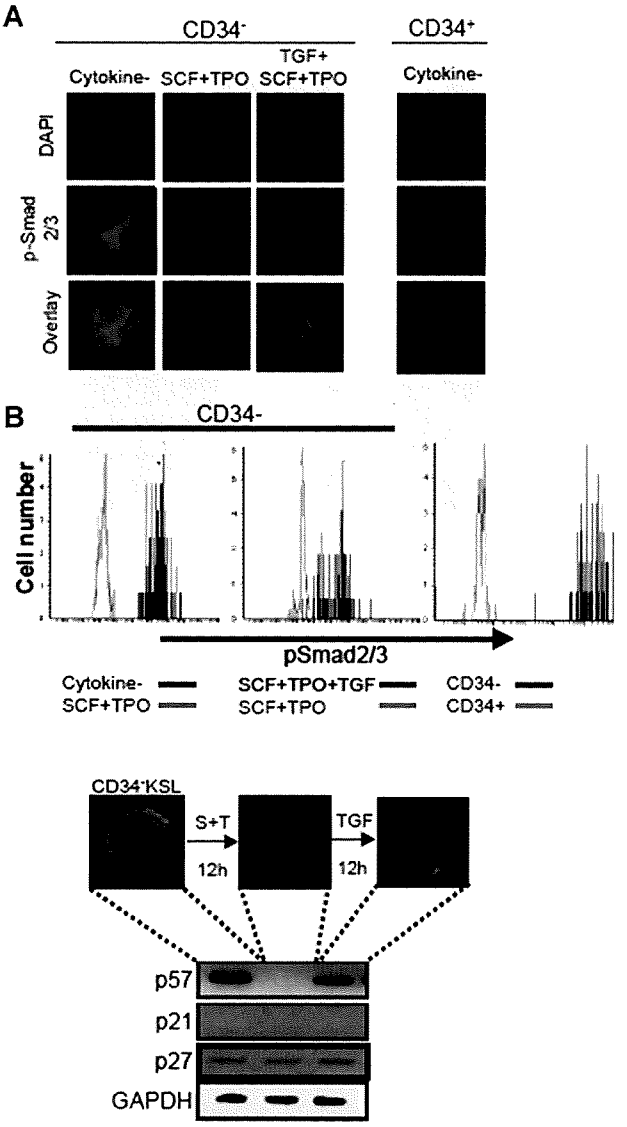

Figure 3. TGF-β signaling is highly active in dormant HSCs and regulates *p57* expression. (A) Active TGF-β signaling in HSCs demonstrated by presence of phosphorylated Smad2/3 in the nucleus. Freshly isolated CD34⁻KSL HSCs (CD34⁻) and CD34⁺KSL hematopoietic progenitor cells (CD34⁺) were sorted in a serum-free culture-medium drop on slide glasses. The sorted cells were incubated at 37°C for 30 minutes in the presence or absence of TGF-β1 and then were stimulated with SCF and TPO for another 30 minutes. Freshly isolated CD34⁺KSL progenitor cells were also subjected to analysis. The cells were stained with DAPI (blue) and an anti–phospho-Smad2/3 antibody (red). Representative images are depicted on the top panels. In the bottom panels, the levels of immunofluorescence quantitated by an Olympus Laser Scanning Cytometer 2 (LSC2) are depicted. X- and y-axes are indicated in logarithmic and linear scales, respectively. The left panel presents data from freshly isolated CD34⁻KSL HSCs (CD34⁻) incubated for 30 minutes in the presence or absence of SCF and TPO. The middle panel presents data from freshly isolated CD34⁻KSL HSCs (CD34⁻) incubated for 30 minutes in the presence or absence of TGF-β1, and then stimulated with SCF and TPO for another 30 minutes. The right panel presents data from freshly isolated CD34⁻KSL HSCs (CD34⁻) and CD34⁺KSL hematopoietic progenitor cells (CD34⁺). (B) TGF-β up-regulates *p57* gene expression in HSCs to induce cell-cycle arrest. Freshly isolated CD34⁻KSL HSCs were incubated in the presence of SCF (S) and TPO (T) for 12 hours, and were cultured for another 12 hours in the presence of TGF-β1 (TGF) in addition to SCF and TPO. The cells were stained with DAPI (blue) and an anti-p57 antibody (green). mRNA expression of mouse *Cip/Kip* genes was analyzed for each cell (bottom panel).

HSCs, although established chimerism declined compared with that established by freshly isolated HSCs. All these data strongly support the proposition that TGF-β induces hibernation in HSCs ex vivo without affecting HSC capacity to self-renew and to differentiate into a full range of hematopoietic cell lineages.

The TGF-β signal is active in hibernating niche HSCs

The activated TGF-β receptor complex phosphorylates Smad2 and Smad3. Smad2 and Smad3 use Smad4 as a partner to form a transcriptionally active complex. To obtain physiologic evidence that supports active TGF-β signaling in niche HSCs, we next examined TGF-β signals in freshly isolated HSCs. Smad2/3, the signaling molecules directly downstream from and activated by TGF-β receptors, were highly phosphorylated in freshly isolated CD34⁻KSL HSCs, where they accumulated in the nucleus. In contrast, Smad2/3 were scarcely phosphorylated in CD34⁺KSL progenitor cells (Figure 3A). Quantification of the levels of Smad2/3 phosphorylation by laser scanning microscopy showed a striking contrast between freshly isolated CD34⁻KSL HSCs and CD34⁺KSL progenitors (Figure 3A). These data strongly indicate that the TGF-β signaling pathway is active in HSCs in the BM niche, but not in progenitor cells. We observed, in keeping with this, that Smad2/3 in HSCs were rapidly dephosphorylated by cytokine stimulation. Pretreatment of HSCs with TGF-β, however, again counteracted cytokine stimulation and Smad2/3 remained phosphorylated (Figure 3A).

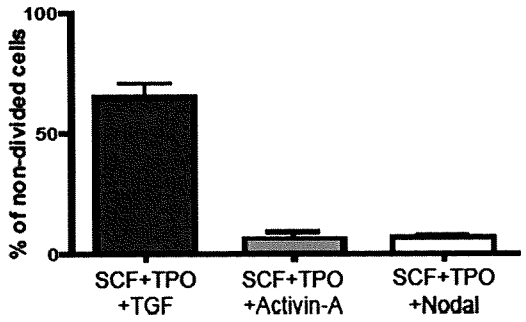

Figure 4. TGF-β, but not other TGF-β family members, confers a cytostatic effect on HSCs ex vivo. Freshly isolated CD34⁻KSL HSCs were sorted clonally into 96-well microtiter plates and incubated in the presence of SCF, TPO, and TGF-β1; SCF, TPO, and Activin-A; or SCF, TPO, and Nodal. At day 2 of culture, nondivided cells that stayed dormant were assessed under an inverted microscope.

We previously reported that CD34⁻KSL HSCs express a high level of *p57*^{Kip2}, whereas CD34⁺KSL progenitor cells do not. Of note was that p57 as well as cyclin D1, D2, and D3 localize in the cytoplasm in HSCs.[9] That TGF-β up-regulates *p57* expression in human primitive hematopoietic cells to induce cell-cycle arrest intrigued us.[20] To verify this finding in mouse HSCs, we stimulated freshly isolated CD34⁻KSL HSCs with SCF and TPO for 12 hours, to down-regulate *p57;* we then treated the cells with TGF-β. Twelve hours after the addition of TGF-β, p57 was abundantly reinduced at both mRNA and protein levels, whereas expression of *p21* and *p27* did not change at all (Figure 3B). These data indicate that TGF-β regulates the expression of p57, which supposedly functions as a specific CDKI that binds to and suppresses the activity of the cyclin D/CDK complexes in HSCs.

TGF-β induces hibernation, but other TGF-β family members do not

Smad2 and Smad3 are activated not only by TGF-β, but also by Activin and Nodal.[21] We evaluated the effects of these agents on HSC cell cycle. Single CD34⁻KSL HSCs were cultured in the presence of SCF, TPO, and Activin or Nodal. TGF-β strongly suppressed division of single HSCs; 65.7% of them stayed dormant during 2-day culture. Activin-A and Nodal were not efficient in suppressing division of single HSCs; they, respectively maintained dormancy in only 6.6% and 6.9% of HSCs during 2-day culture (Figure 4). These data establish that within its family TGF-β has a major role in maintenance of HSC hibernation.

Activation of latent TGF-β is required for TGF-β bioactivity

TGFβ reportedly is produced not only by niche cells, but also by HSCs themselves.[7] As expected, HSCs expressed a significant level of *TGF-β1* and a low level of *TGF-β3,* but not *Activin A* or *Nodal,* indicating the presence of both autocrine and paracrine regulatory loops of TGF-β signaling (Figure 5A). Importantly, however, TGF-β is produced as an inactive form, latent TGF-β. We asked whether HSCs themselves could activate latent TGF-β to establish an autocrine TGF-β signaling loop. We seeded single CD34⁻KSL HSCs in the presence of SCF and TPO along with either active-form TGF-β or latent TGF-β, and allowed the HSCs to form colonies. TGF-β strongly suppressed colony formation, whereas latent TGF-β did not affect colony formation at all. These data indicate that HSCs can produce latent TGF-β but cannot activate it by themselves. Since TGF-β is produced by a variety of cells as an inactive form, the capacity to activate latent TGF-β could be a key property of BM niche cells.

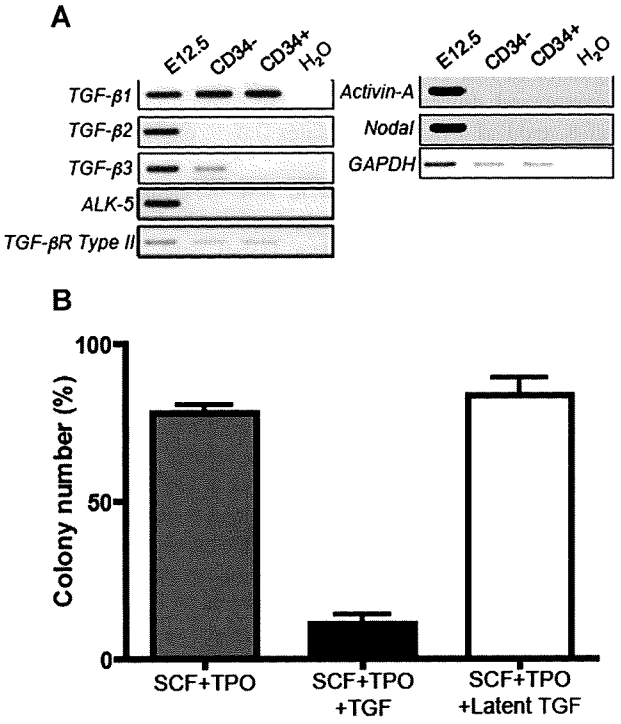

Figure 5. Activation of latent TGF-β is required for TGF-β bioactivity on HSCs. (A) mRNA expression of TGF-β family member genes was analyzed for total embryo at E12.5, freshly isolated BM CD34⁻KSL HSCs (CD34⁻), and CD34⁺KSL hematopoietic progenitor cells (CD34⁺). (B) Freshly isolated CD34⁻KSL HSCs (CD34⁻) were sorted clonally into 96-well microtiter plates and incubated in the presence of SCF and TPO along with either TGF-β1 or latent TGF-β1, and were allowed to form colonies. After 14 subsequent days of culture, the numbers of colonies were counted and the percentages of starting HSCs that gave rise to colonies were presented.

Discussion

The cell-cycle status of HSCs in the niche is supposed to be precisely regulated by a specific combination of niche signals. We have reported an unexpected role of lipid raft organization in the maintenance of HSC hibernation through regulating the PI3K-Akt-FoxO pathway that lies downstream of cytokine signaling.[9] HSCs are exposed to a variety of secreted and membrane-bound growth factors in the niche. Nonetheless, our findings clearly demonstrate that lipid raft reorganization is strictly inhibited in HSCs in the niche. We inferred that nonclustered lipid raft microdomains finely tune cytokine signals and mediate them toward suitability for HSC survival in the hibernating state, and that some niche signals inhibit lipid raft reorganization to maintain HSC hibernation. These findings support a novel model in which HSC fate, that is, hibernation or cell-cycle re-entry, largely depends on lipid raft regulation.

We have now identified that TGF-β inhibits cytokine-induced LRC (Figure 1A). TGF-β suppresses Akt activation and induces nuclear accumulation of FoxO3a in HSCs. It also inhibits translocation of cyclin D1 into the nucleus and maintains high cytoplasmic accumulations of p57 (Figure 1D and data not shown). Through these mechanisms, TGF-β strongly inhibits cell division and maintains HSCs in the hibernating state ex vivo. Together with our finding that Smad2 and Smad3, which are activated by the TGFβ receptor complex, are selectively and highly phosphorylated in CD34⁻KSL HSCs, but not in CD34⁺KSL progenitor cells, these findings strongly indicate a physiologic role for TGF-β in HSC hibernation in the

niche (Figure 3A). This notion is also supported by the study of *C elegans,* which indicated a critical role of Daf-7 as a positive regulator of Daf-16.[22] Daf-7 is a TGF-β–like molecule. Via its receptor and downstream signaling molecules (Daf-4, Daf-1, Daf-8, and Daf-14), it up-regulates Daf-16 expression and exerts a dauer larval gene program.[23]

TGF-β is widely expressed in BM by elements that include osteoblasts and other stromal cells. Importantly, however, TGF-β is produced as a latent form. Latent TGF-β must be processed and activated. As shown in Figure 5B, HSCs are not able to activate latent TGF-β. That the BM niche is where TGF-β can be processed/activated and where TGF-β induces HSC hibernation is thus a tempting hypothesis. In contrast, Ang-1, another regulator of HSC hibernation, was much less effective than TGF-β in inhibiting cytokine-induced LRC and subsequent Akt activation (data not shown). Recently, the TPO signal was proposed as an essential component for HSC hibernation in the osteoblastic niche.[24] TPO efficiently induces LRC and activates the PI3K-Akt pathway in vitro. However, its signal is supposedly attenuated by inhibited LRC in hibernating HSCs in the niche. We assume that the attenuated TPO signal by inhibitory niche signals including TGF-β acts as a survival signal but not proliferation signal on HSCs and holds the key in keeping HSCs in hibernation. These data highlight lipid raft assembly and its regulation by TGF-β as a novel regulatory component of HSC hibernation. Our findings thus indicate that HSC hibernation is regulated by at least 2 different routes, the Ang-1–Tie-2 and TGF-β–Smad signaling pathways, and establish a central role for TGF-β in regulating the lipid raft–PI3K–Akt–FOXO pathway.

Although TGF-β has been well characterized as a negative regulator of hematopoietic stem and progenitor cell proliferation in vitro,[7] mice models deficient for TGF-β signaling molecules, including ALK-5 TβRI, show no defects in maintenance or quiescence of HSCs.[17] These discrepancies may be at least partly explained by the considerably low mRNA expression of ALK-5 in HSCs compared with that in E12.5 total embryo (Figure 5A), which is indicative of alternative TβRIs in HSCs. Mice deficient for the TβRII have not been well characterized with respect to HSC hibernation because of lethal inflammatory disorder affecting multiple organs.[16] Furthermore, overlapping receptor and Smad usage by different TGF-β superfamily ligands (TGF-βs, BMPs, and Activins) accounts for their functional redundancies, making their signals more complicated in vivo than is seen in liquid cultures ex vivo. Of note is that Smad4, which acts at a common level of convergence for all TGF-β superfamily signals, has recently been identified as critical for maintenance of self-renewing HSCs.[25] Thus, the physiological role of the TGF-β awaits further evaluation.

The negative regulation of lipid raft assembly is poorly understood. In this regard, the direct inhibition of lipid raft reorganization by TGF-β is notable. In the present study, TGF-β significantly inhibited cytokine-induced activation of c-Src, one of the lipid raft components, in HSCs (Figure 1B). This effect was comparable with that exerted by PP2, an inhibitor specific for Src-family kinases (Figure S1). Intriguingly, TGF-β has been reported to down-regulate protein expression of Src-family kinases.[26,27] Although the precise mechanism whereby TGF-β inhibits c-Src activation remains obscure, Src-family kinases could be key targets for TGF-β in affecting lipid raft reorganization.

TGF-β reportedly induces cell cycle arrest through up-regulating CDKIs, including p15INK4B (p15), p21, and p27, in various cell types.[28,29] However, TGF-β has been demonstrated to induce growth arrest in HSCs independently of p21 or p27.[30] We here have presented evidence that TGF-β specifically up-regulates the expression of *p57*, but not *p15, p21,* or *p27,* in HSCs (Figure 3B and data not shown). In accord with our findings, *p57* has been identified as the only CDKI significantly up-regulated by TGF-β in vitro in human $CD34^+$ primitive hematopoietic cells; of importance was the observation that knockdown of *p57* expression blocked the cytostatic effect of TGF-β.[20] All these findings indicate the importance of TGF-β in regulating *p57* expression and in maintaining HSC hibernation.

In this study, we also evaluated the role of autocrine TGF-β signaling loop in HSCs. Our data indicated that HSCs can produce latent TGF-β but cannot activate it by themselves. Latent TGF-β does not affect HSC cell growth at all. Intriguingly, a cell cycle–independent role of autocrine TGF-β has been reported on human primitive hematopoietic progenitor cells under a culture condition without supporting cells that can activate latent TGF-β.[31] Whether the latent TGF-β can transduce alternative signals via an as-yet-unrecognized pathway in HSCs is a tempting question to be addressed.

Our findings stress the critical role of lipid rafts in regulating the cell-cycle status of HSCs and demonstrate a novel interplay between the lipid raft–PI3K–Akt–FoxO and the TGF-β–Smad signaling pathways in HSCs hibernating in the BM niche. Smad proteins activated by TGF-β could form a complex with FoxO proteins FoxO1, FoxO3a, and FoxO4.[32] TGF-β–mediated interaction between these 2 signaling pathways thus could hold a key role in the regulation of gene expression that controls HSC hibernation.

Acknowledgments

We thank Y. Morita and Y. Yamazaki for technical help and advice and Dr A. S. Knisely for critical reading of the paper.

This work was supported in part by grants from the Ministry of Education, Culture, Sport, Science and Technology, Japan, Japan Science and Technology Corporation (JST), the Naito Foundation (Tokyo, Japan), and the Terumo Lifescience Foundation (Kanagawa, Japan).

Authorship

Contribution: S.Y., A.I., and H.E. designed the research and analyzed data; S.Y., A.I., and H.N. wrote the paper; K.E. contributed vital new reagents; and S.Y. and S.T. performed research and analyzed data.

Conflict-of-interest disclosure: The authors declare no competing financial interests.

Correspondence: Hiromitsu Nakauchi, 4-6-1 Shirokanedai, Minato-ku, Tokyo, Japan; e-mail: nakauchi@ims.u-tokyo.ac.jp.

References

1. Cheshier SH, Morrison SJ, Liao X, Weissman IL. In vivo proliferation and cell cycle kinetics of long-term self-renewing hematopoietic stem cells. Proc Natl Acad Sci U S A. 1999;96:3120-3125.
2. Sudo K, Ema H, Morita Y, Nakauchi H. Age-associated characteristics of murine hematopoietic stem cells. J Exp Med. 2000;192:1273-1280.
3. Taichman RS. Blood and bone: two tissues whose fates are intertwined to create the hematopoietic stem-cell niche. Blood. 2005;105:2631-2639.
4. Arai F, Hirao A, Ohmura M, et al. Tie2/angiopoietin-1 signaling regulates hematopoietic stem cell quiescence in the bone marrow niche. Cell. 2004; 118:149-161.
5. Calvi LM, Adams GB, Weibrecht KW, et al. Osteoblastic cells regulate the haematopoietic stem cell niche. Nature. 2003;425:841-846.
6. Zhang J, Niu C, Ye L, et al. Identification of the haematopoietic stem cell niche and control of the niche size. Nature. 2003;425:836-841.

7. Larsson J, Karlsson S. The role of Smad signaling in hematopoiesis. Oncogene. 2005;24:5676-5692.
8. Osawa M, Hanada K, Hamada H, Nakauchi H. Long-term lymphohematopoietic reconstitution by a single CD34-low/negative hematopoietic stem cell. Science. 1996;273:242-245.
9. Yamazaki S, Iwama A, Takayanagi S, et al. Cytokine signals modulated via lipid rafts mimic niche signals and induce hibernation in hematopoietic stem cells. EMBO J. 2006;25:3515-3523.
10. Jahn T, Seipel P, Urschel S, Peschel C, Duyster J. Role for the adaptor protein Grb10 in the activation of Akt. Mol Cell Biol. 2002;22:979-991.
11. Coffer PJ, Burgering BM. Forkhead-box transcription factors and their role in the immune system. Nat Rev Immunol. 2004;4:889-899.
12. Greer EL, Brunet A. FOXO transcription factors at the interface between longevity and tumor suppression. Oncogene. 2005;24:7410-7425.
13. Tothova Z, Kollipara R, Huntly BJ, et al. FoxOs are critical mediators of hematopoietic stem cell resistance to physiologic oxidative stress. Cell. 2007;128:325-339.
14. Miyamoto K, Araki KY, Naka K, et al. Foxo3a is essential for maintenance of the hematopoietic stem cell pool. Cell Stem Cell. 2007;1:101-112.
15. Shull MM, Ormsby I, Kier AB, et al. Targeted disruption of the mouse transforming growth factor-beta 1 gene results in multifocal inflammatory disease. Nature. 1992;359:693-699.
16. Levéen P, Larsson J, Ehinger M, et al. Induced disruption of the transforming growth factor β type II receptor gene in mice causes a lethal inflammatory disorder that is transplantable. Blood. 2002;100:560-568.
17. Larsson J, Blank U, Helgadottir H, et al. TGF-beta signaling-deficient hematopoietic stem cells have normal self-renewal and regenerative ability in vivo despite increased proliferative capacity in vitro. Blood. 2003;102:3129-3135.
18. Ema H, Morita Y, Yamazaki S, et al. Adult mouse hematopoietic stem cells: purification and single-cell assays. Nat Protoc. 2006;1:2979-2987.
19. Osawa M, Yamaguchi T, Nakamura Y, et al. Erythroid expansion mediated by the Gfi-1B zinc finger protein: role in normal hematopoiesis. Blood. 2002;100:2769-2777.
20. Scandura JM, Boccuni P, Massague J, Nimer SD. Transforming growth factor beta-induced cell cycle arrest of human hematopoietic cells requires p57KIP2 up-regulation. Proc Natl Acad Sci U S A. 2004;101:15231-15236.
21. Waite KA, Eng C. From developmental disorder to heritable cancer: it's all in the BMP/TGF-beta family. Nat Rev Genet. 2003;4:763-773.
22. Ogg S, Paradis S, Gottlieb S, et al. The Fork head transcription factor DAF-16 transduces insulin-like metabolic and longevity signals in C. elegans. Nature. 1997;389:994-999.
23. Inoue T, Thomas JH. Suppressors of transforming growth factor-beta pathway mutants in the Caenorhabditis elegans dauer formation pathway. Genetics. 2000;156:1035-1046.
24. Yoshihara H, Arai F, Hosokawa K, et al. Thrombopoietin/MPL signaling regulates hematopoietic stem cell quiescence and interaction with the osteoblastic niche. Cell Stem Cell. 2007;1:685-697.
25. Karlsson G, Blank U, Moody JL, et al. Smad4 is critical for self-renewal of hematopoietic stem cells. J Exp Med. 2007;204:467-474.
26. Atfi A, Drobetsky E, Boissonneault M, Chapdelaine A, Chevalier S. Transforming growth factor beta down-regulates Src family protein tyrosine kinase signaling pathways. J Biol Chem. 1994;269:30688-30693.
27. Park SS, Eom YW, Kim EH, et al. Involvement of c-Src kinase in the regulation of TGF-beta1-induced apoptosis. Oncogene. 2004;23:6272-6281.
28. Cheng T, Rodrigues N, Shen H, et al. Hematopoietic stem cell quiescence maintained by p21cip1/waf1. Science. 2000;287:1804-1808.
29. Ezoe S, Matsumura I, Satoh Y, Tanaka H, Kanakura Y. Cell cycle regulation in hematopoietic stem/progenitor cells. Cell Cycle. 2004;3:314-318.
30. Cheng T, Shen H, Rodrigues N, Stier S, Scadden DT. Transforming growth factor beta 1 mediates cell-cycle arrest of primitive hematopoietic cells independent of p21(Cip1/Waf1) or p27(Kip1). Blood. 2001;98:3643-3649.
31. Pierelli L, Marone M, Bonanno G, et al. Modulation of bcl-2 and p27 in human primitive proliferating hematopoietic progenitors by autocrine TGF-beta1 is a cell cycle-independent effect and influences their hematopoietic potential. Blood. 2000;95:3001-3009.
32. Seoane J, Le HV, Shen L, Anderson SA, Massague J. Integration of Smad and forkhead pathways in the control of neuroepithelial and glioblastoma cell proliferation. Cell. 2004;117:211-223.